1 **Label-free lymphocytes reconstitution using side scatter for**

2 **optimal T cell manufacturing**

3

4 **Tongjin Wu[1], Yen Hoon Luah[1], Yongqiang Luo[1], Howard John Womersley[1],**

5 **Lih Feng Cheow[1,2,*]**

6

7 [1]Department of Biomedical Engineering, Faculty of Engineering, National University

8 of Singapore, Singapore 117583, Singapore.

9 [2]Institute for Health Innovation and Technology, National University of Singapore,

10 Singapore 117599, Singapore.

11 [*]Correspondence: lihfeng.cheow@nus.edu.sg

12

13

14

15

16

17

18

19

20

21

22

23 **SUMMARY**

24 Lymphocyte biology research commonly involves purification of lymphocyte

25 subpopulations by fluorescence-activated cell sorting (FACS) or immunomagnetic

26 separation (IMS), both of which typically rely on antibody labeling of validated cell

27 markers. Methods enabling label-free segregation of lymphocyte subpopulations

28 would be invaluable with regard to less-perturbation, simplicity and cost-effectiveness.

29 Here, we introduce TRuST, a label-free approach for T cell reconstitution using side-

30 scatter (SSC). TRuST-sorted SSC^{low} cells enrich for CD4$^+$ T and naïve T cells, while

31 SSC^{high} cells enrich for CD8$^+$ T, NK and differentiated T cells. Enrichment purity can be

32 improved by computational gate design. SSC^{low} cells have superior expansion capacity

33 and generate more central memory precursors with naïve-resembling cytokine

34 responses. Moreover, we find that both T cell differentiation status and CD4/CD8 T

35 ratio in the starting cellular material are critical attributes predicting T cell product

36 quality and quantity. TRuST presents an effective and reliable technique for label-free

37 lymphocytes selection and reconstitution.

38

39 **Keywords:** flow cytometry; side scatter; antibody-free; label-free; cell type purification;

40 T cell reconstitution; naïve T cell enrichment; ratio of CD4/CD8 T; T cell manufacturing

41

42 **INTRODUCTION**

43 Lymphocytes, mainly including T cells, natural killer (NK) cells and B cells, play an

44 indispensable part in human immune system. Use of purified lymphocyte subsets for

45 lymphocyte biology research is critical to dissect the functional heterogeneity of

46 lymphocyte subpopulations. Fluorescence-activated cell sorting (FACS) (Cossarizza

47 et al., 2019) and immunomagnetic separation (IMS) (Plouffe et al., 2015) are methods

48 of choice to obtain purified cell types of interest, relying on the labeling with specific

49 antibody conjugates such as fluorochrome-modified antibodies and magnetic beads-

50 coupled antibodies. Despite powerful of these technologies, there still exist some

51 limitations.

52

53 One of the most common concerns is antibody labeling-caused functional change of

54 immune cells which are relatively sensitive to antibody-mediated activation/inhibition

55 (Attanasio and Wherry, 2016; Chen and Flies, 2013),   interfering with downstream cell

56 biology studies. Thus, careful selection of validated antibody clones and strict

57 experimental controls are generally required in experimental design. In addition, it is

58 extremely difficult to release the bound fluorescent antibodies on cell surface if cell

59 viability was to be maintained. These sorted cells are not suitable for re-labeling with

60 the same fluorochrome conjugates due to occupancy of fluorescence channels,

61 resulting in less flexibility in the choice of fluorescent antibodies for multiparametric

62 flow cytometry experiments. Also, these cells might not be feasible for downstream cell

63 culture assays if the occupied target markers were necessary to be re-engaged for cell

64 functionality. For example, the labeling of CD3 receptor for T cells enrichment by FACS

65 might affect the activation/expansion of T cells when CD3/CD28 engagement is

66 required for cell stimulation (Roddie et al., 2019). Superparamagnetic particles-

3

67 antibody coupling technique combined with magnetic isolation is shown to be capable

68 of minimizing the effects introduced by fluorescent antibodies occupancy thanks to its

69 effective separation with only unsaturated concentration of bead-antibody conjugates

70 (Grutzkau and Radbruch, 2010; Plouffe et al., 2015). However, concerns arising from

71 the use of nanosized magnetic beads include internalization of magnetic beads and

72 preservation of magnetic properties for an extended period in cells that are subjected

73 to limited proliferation, which calls for caution when repetitive positive isolation steps

74 after in vitro culture are required (Laghmouchi et al., 2020; Teeman et al., 2019). More

75 recently, Miltenyi Biotec has introduced the REAlease Fluorochrome Technology that

76 relies on engineered antibody fragments with low epitope binding affinities which

77 allows stained antibodies to be released. Design of releasable superparamagnetic

78 beads-antibody conjugate could be of interest to improve magnetism-based cell

79 separation. Nevertheless, the time and cost for sample processing are inevitably

80 increased and concerns relating to cell labeling-caused alteration on downstream

81 assays still exist. Therefore, with regard to less perturbation on target cells and

82 enhanced flexibility in sample processing, approaches that enable label-free cell type

83 separation from mixed lymphocytes would be highly attractive and great useful in

84 lymphocyte biology studies.

85

86 Selection of specific T cell types has also seen its utility in the field of cellular

87 immunotherapy. Insight into attributes of therapeutic potency based on T cell receptor

88 (TCR)-redirected T cells such as chimeric antigen receptor (CAR) T cells and TCR-T

89   cells is a central goal of T cell immunotherapy (Majzner and Mackall, 2019; Rafiq et al.,

90   2020). The quality of T cell products generated ex vivo has been recognized as a

91   critical factor affecting immunotherapy efficacy (Deng et al., 2020; Finney et al., 2019;

92   Fraietta et al., 2018; Roddie et al., 2019). Unfractionated peripheral blood mononuclear

93   cell (PBMC) concentrates are commonly used for T cell production, leading to

94   uncontrollable batch-to-batch variation. Separate expansion of CD4+ T and CD8+ T

95   cells pre-enriched by immunomagnetic selection enhances product consistency and

96   manufacturing feasibility (Gardner et al., 2017; Shah et al., 2020; Sommermeyer et al.,

97   2016; Turtle et al., 2016). Of note, CD4+ T cells help is critical for shaping the adaptive

98   immunity of CD8+ T cells in vivo (Nakanishi et al., 2009; Sun et al., 2004) and improves

99   CD8+ T cells tumor-eradicating potency (Alspach et al., 2019; Arina et al., 2017;

100   Nakanishi et al., 2009; Schietinger et al., 2010). However, the notion, whether CD4+ T

101   and CD8+ T cells should be expanded separately or together at designed ratio in vitro,

102   especially in the scenario where external antigens are absent, remains to be clarified.

103   In addition, adoptive transfer of T cell products derived from less-differentiated T cell

104   subsets shows better curative potential than their more-differentiated counterparts as

105   observed in both animal works (Berger et al., 2008; Gattinoni et al., 2011; Hinrichs et

106   al., 2009; Hinrichs et al., 2011; Wang et al., 2011) and clinical studies (Finney et al.,

107   2019; Fraietta et al., 2018; Xu et al., 2014). These studies suggest that preselecting

108   specific T cell subtypes would be very useful for cell manufacturing aiming to improve

109   immunotherapy efficacy. Undoubtedly, increased demand for therapeutic T cell product

110   calls for cost-effectiveness and manufacturing simplicity. Methods enabling the

5

111 segregation of ideal cell subsets without the use of costly antibodies would be

112 invaluable by omitting the requirement of large amount of clinical grade

113 immunomagnetic antibodies and complicated downstream processing workflows.

114

115 There has been an increasing number of thought-provoking studies on label-free

116 lymphocytes identification. Light scattering, a parameter commonly used in flow

117 cytometry, is capable of measuring cell size via forward scatter (FSC) and cellular

118 granularity by side scatter (SSC) (Cossarizza et al., 2019). Light scattering has already

119 seen its versatile applications in the screening of lymphocyte samples to distinguish

120 healthy and disease patients such us B-cell chronic lymphocytic leukemia (B-CLL)

121 (Terstappen et al., 1988), cutaneous T-cell lymphoma (Clark et al., 2011) and chronic

122 hepatitises B or C infection (Ruban et al., 2010). The principle underlining light

123 scattering relied disease diagnostics could be that, in general, CD8$^+$ T cells has higher

124 SSC than CD4$^+$ T cells while B cells tend to locate between the resting and activated

125 CD8$^+$ T cells populations (Terstappen et al., 1986a; Terstappen et al., 1986b). Of note,

126 most of the reports have not clearly clarified the potential confounding effects resulting

127 from cell size on SSC pattern given that unhealthy or activated lymphocytes with

128 altered size (higher FSC) are likely to change their SSC profile also (Clark et al., 2011;

129 Loudon et al., 1988; Terstappen et al., 1988). Thus, the question arising is whether

130 SSC distribution is enough to tell the differences of lymphocyte cell types that have

131 indistinguishable cell size, for example, healthy lymphocyte subpopulations under

132 resting status. Moreover, to date, a closer look at the subtle scattering distribution of T

6

133   cell differentiation lineages (e.g. naïve/memory T cells) has been neglected.

134   Memory/effector T cells are observed to have more granules than their naïve

135   counterparts under transmission electron microscope (Dimeloe et al., 2016). These

136   findings imply that cell general biophysical attributes (e.g. light scattering) may be

137   further exploited to select for lymphocyte subpopulations with particular functionality,

138   such as for immunotherapy.

139

140   Taken together, these inadequacies highlight the need for new methods capable of

141   selecting lymphocyte subpopulations in a label-free manner by relying on general cell

142   biophysical properties. To achieve this, we initially had an in-depth analysis of the light

143   scattering profile (FSC/SSC) of resting human lymphocyte subsets, including NK cells,

144   B cells, total CD4$^+$ T cells, total CD8$^+$ T cells, as well as CD4$^+$ or CD8$^+$ naïve/memory

145   T cell subsets. We found that SSC instead of FSC is a robust biophysical property to

146   distinguish lymphocyte subsets. Generally, lymphocytes with "helper" function such as

147   CD4$^+$ T cells and B cells have a lower SSC than that with "cytotoxic" function such as

148   CD8$^+$ T cells and NK cells. Interestingly, this discrepancy in SSC profile is even more

149   apparent among T cell differentiation lineages regardless of CD4$^+$ or CD8$^+$ T cell type.

150   Younger T cells such as naïve T cells and memory precursors have a significantly lower

151   SSC than their more-differentiated counterparts including central memory T cells,

152   effector memory T cells and terminally effector memory T cells. Inspired by these

153   findings, we developed TRuST, a label-free method for T cell reconstitution using side

154   scatter. TRuST-relied T cell segregation is based on two gating strategies. One is

155   computational gate search aimed to maximize the purity of target cell type of interest.

156   The other is manual gate selection which is easier and more flexible in reconstituting

157   lymphocyte composition instead of focusing on single cell subset. We further

158   demonstrated that reconstituted SSC^{low} cells that are enriched for $CD4^+$ T and naïve T

159   cells have superior expansion capacity and produce more central memory precursors.

160   Finally, using the TRuST-based T cell segregation, we were able to find that both less-

161   differentiated T cell subpopulations and high $CD4^+$ T to $CD8^+$ T ratio in starting cellular

162   material are critical attributes predicting T cell product quality and quantity. This study

163   established TRuST as an effective and reliable technique for label-free lymphocytes

164   selection and reconstitution, which would be useful for lymphocytes biology studies

165   and T cell manufacturing for improved immunotherapy.

166

167   **RESULTS**

168   **TRuST development**

169   TRuST is a label-free approach for lymphocyte subpopulations selection and T cell

170   reconstitution. The development of TRuST was inspired by the intrinsic side-scattering

171   difference of lymphocyte subpopulations including $CD4^+$ T cells, $CD8^+$ T cells, NK cells,

172   B cells, and main T cell differentiation lineages including naïve (T_N, $CD45RA^{high}$

173     $CCR7^{high}$), central memory (T_{CM}, $CD45RA^{dim/-}$ $CCR7^{low}$), effector memory (T_{EM},

174     $CD45RA^{dim/-}$ $CCR7^-$) and terminally differentiated effector (T_{EMRA}, $CD45RA^{high}$ $CCR7^-$)

175   (**Figures 1A, S1A, and S1B**) (Bohler et al., 2007; Seder and Ahmed, 2003). Due to

176   the heterogeneous SSC patterns of lymphocyte subpopulations, using the pre-stained

8

177   lymphocytes for each new sample, it is feasible to find the optimum gate that has the

178   desired purity and yield for target cells of interest via GateID, a computational gate

179   search algorithm for cell type purification (Baron et al., 2019) (**Figure 1B**). Alternatively,

180   a series of manual gates can be set to determine the optimum gate for T cell

181   reconstitution depending on the research aims (**Figure 1C**). The selected gate can be

182   simply adopted and applied for the sorting of unstained lymphocytes (**Figure 1D**). For

183   downstream cell culture assays such as T cell expansion for immunotherapy, the total

184   lymphocytes can be directly sorted into SSC^{low} and SSC^{high} groups that consist of

185   functionally distinct T cell subsets. The sorted cells are subjected to canonical

186   expansion protocol using anti-CD3/CD28 microbeads plus interleukin-2 (IL-2) (**Figures**

187   **1D and 1E**). This enables us to study how the initial cell composition affect T cell

188   expansion dynamics, phenotypes formation, and functionality shaping in

189   multifunctional cytokine expression (**Figures 1E and S1C**), and the attributes that

190   contribute to the discrepancies of final T cell products (**Figure 1E**). Together, this work

191   flow demonstrates the utility of TRuST for label-free lymphocyte selection and T cell

192   constitution for downstream lymphocytes biology study.
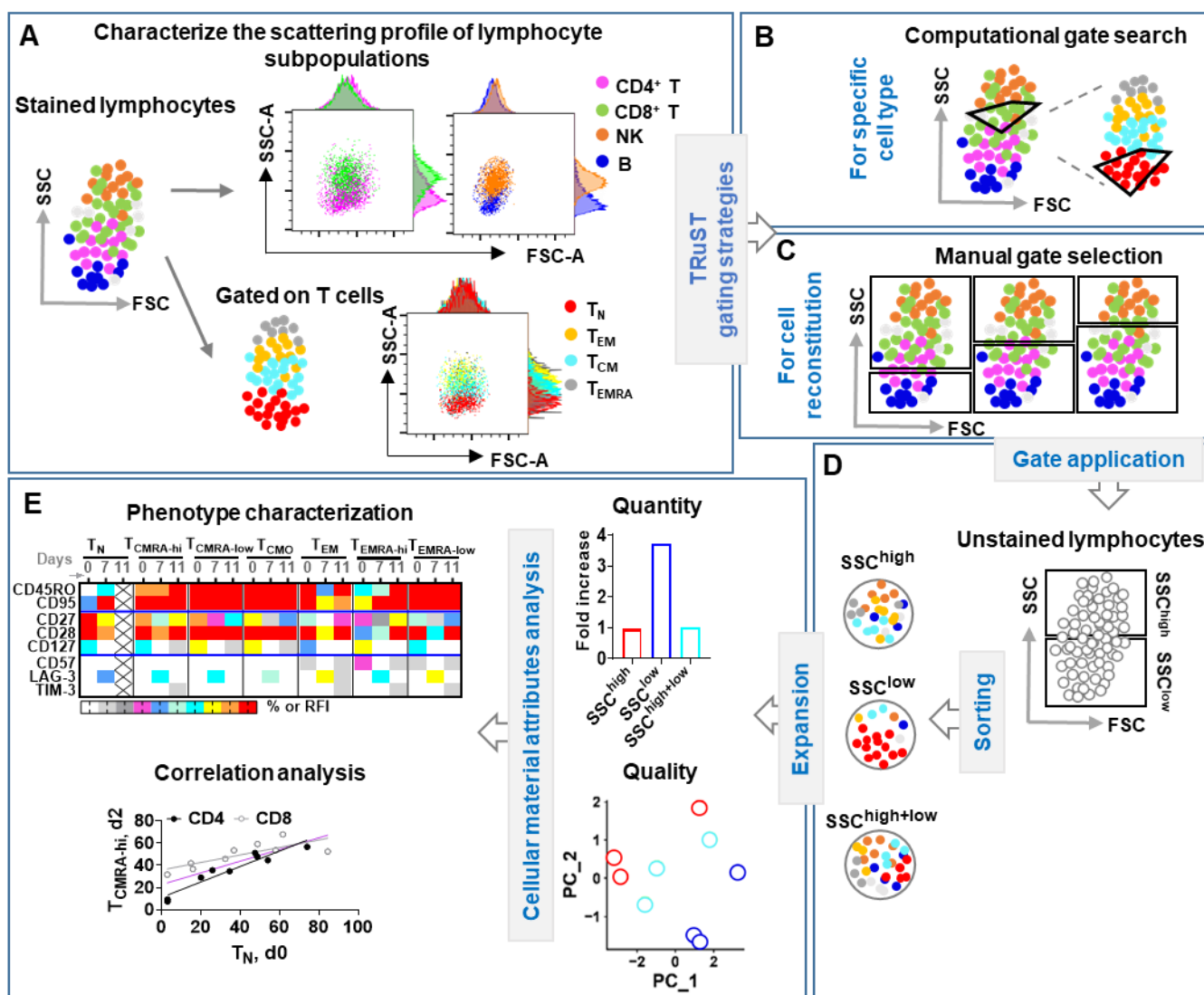
193   (main text continued after Figure 1)

194 **Figure 1. TRuST: An effective approach for label-free T cell selection and reconstitution**

195 (**A**) PBMC samples were stained with lymphocyte subpopulation-representing fluorescence

196 antibodies. Data was acquired by flow cytometer and the forward/side-scattering (FSC/SSC)

197 distribution of main lymphocyte populations and T cell naïve/memory subsets were studied.

198 (**B**) Based on the FSC/SSC profile of lymphocyte populations, a computational gate design

199 algorithm was performed to enrich specific target cell type with optimal purity and yield.

200 (**C**) Alternatively, a manual gating strategy relied on the SSC intensity was used to reconstitute

201 lymphocyte populations with distinct functionality.

10

202   (**D**) The manually selected gate was applied for the sorting of unstained lymphocytes for

203   optimum T cell production.

204   (**E**) A comprehensive comparison of the quantity and quality of T cell products that were derived

205   from cellular materials with different SSC intensity. Characterization of factors contributing to

206   the distinct products by longitudinally phenotypic assessment and correlation analysis.

207   See also **Table S1** and **Methods**.

208

209   **TRuST enables effective reconstitution of functionally distinct lymphocyte**

210   **subpopulations**

211   Lymphocyte cluster can be robustly separated from monocytes and granulocytes

212   based on their FSC/SSC distribution as has been routinely used in flow cytometry.

213   However, a comprehensive study of the subtle scattering profile within various

214   lymphocyte subpopulations is still absent (**Figure 1A**). Using human lymphocytes pre-

215   stained with cell type markers, we found that $CD4^+$ T, B cells and T_N have a lower SSC

216   (low granularity) compared to $CD8^+$ T, NK and differentiated T cells such as T_{CM}, T_{EM}

217   and T_{EMRA} (high granularity) (**Figures 2A and 2B**). With the gradual increase of SSC

218   intensity, there are more $CD8^+$ T and NK cells, as well as more differentiated T cell

219   subsets, leading to percentage reduction of $CD4^+$ T and T_N cells (**Figure S2**). For

220   consistency throughout this work, we manually dived the total lymphocytes into two

221   equal parts (SSC^{high} and SSC^{low}). This gating method is robust enough to either sample

222   staining procedures (**Figures S3A and S3B**) or voltages change applied during flow

223   cytometry data acquiring (**Figures S3A, S3C, and S3D**). On the contrary, FSC can

11

224   only differentiate B cells from NK cells (**Figures S3E-S3G**). The nearly unaltered light

225   scattering profiles between stained and unstained cells (**Figure S3B**) enable us to

226   directly apply the gate in sorting of unstained lymphocytes (**Figure 2C**). Similarly,

227   sorted SSC^{low} group enriches for CD4$^+$ T cells and naïve T cells while SSC^{high} cluster

228   enriches for CD8$^+$ T, NK and other more-differentiated T cell counterparts including T$_{CM}$,

229   T$_{EM}$ and T$_{EMRA}$ (**Figures 2D-2G**). Deep-ultraviolet light (UV) has been adopted for label-

230   free molecular imaging (Zeskind et al., 2007) and hematology analysis (Ojaghi et al.,

231   2020) thanks to its shorter wavelength. Thus, it is interesting to study whether UV light

232   (e.g. UV405 nm) can be used to further improve the scattering resolution of cell

233   morphometric structure under blue light (e.g. B488 nm). However, we observed that a

234   double side-scatter (UV405/B488) based sorting strategy (**Figure S3H**) did not

235   improve the general segregation efficiency of CD4/CD8 T cells, NK/B cells and

236   naïve/memory T cells as well (**Figures S3I-S3M**). Therefore, global cellular granularity,

237   as represented by SSC intensity, could be a general biophysical property used for the

238   separation of lymphocyte subpopulations.

239

240   Next, we sought to characterize the phenotypes of sorted cell populations based solely

241   on SSC intensity. The sorted SSC^{low} cells displayed a higher expression of

242   costimulatory receptors such as CD27 and CD28 but a lower expression of

243   differentiation marker CD127, memory marker CD45RO and activation/inhibition

244   factors CD95/CD57 (**Figure 2H**), consistent with a larger number of naïve T cells in

245   this cell cluster. Unexpectedly, T cells of the same differentiation lineage but different

12

246   SSC intensity also manifested some distinguishable phenotypic traits (**Figures 2I and**

247   **2J**). For example, either T_N or T_{CM} in SSC^{low} group had reduced CD127, CD95 and to

248   a less extent CD57 (**Figure 2I**). Instead, T_{CM} of SSC^{low} cluster had increased CD27

249   (**Figure 2I**) and CCR7/CD45RA abundance (**Figure 2J**), suggesting its central memory

250   precursor-like phenotype. Functionally, in response to short pulse of protein kinase C

251   (PKC) stimulus, the SSC^{low} lymphocytes produced a large amount of IL-2 but reduced

252   IFN-γ-involved immediate effector cytokines (**Figures 2K and 2L**), resembling

253   cytokine expression dynamics of early-differentiated T cells (Denton et al., 2011;

254   Hinrichs et al., 2009). The large amount of IFN-γ but near absence of IL-2 expression

255   in non-T lymphocytes of SSC^{high} group is in line with a high proportion of NK cells in

256   this cluster (**Figures 2M and 2E**). Taken together, these findings suggest that younger

257   T cell lineages including naïve T cells and central memory precursors are intrinsically

258   endowed with a lower SSC, which, concurrently with a higher ratio of CD4$^+$ T to CD8$^+$

259   T cells can be effectively enriched by TRuST.

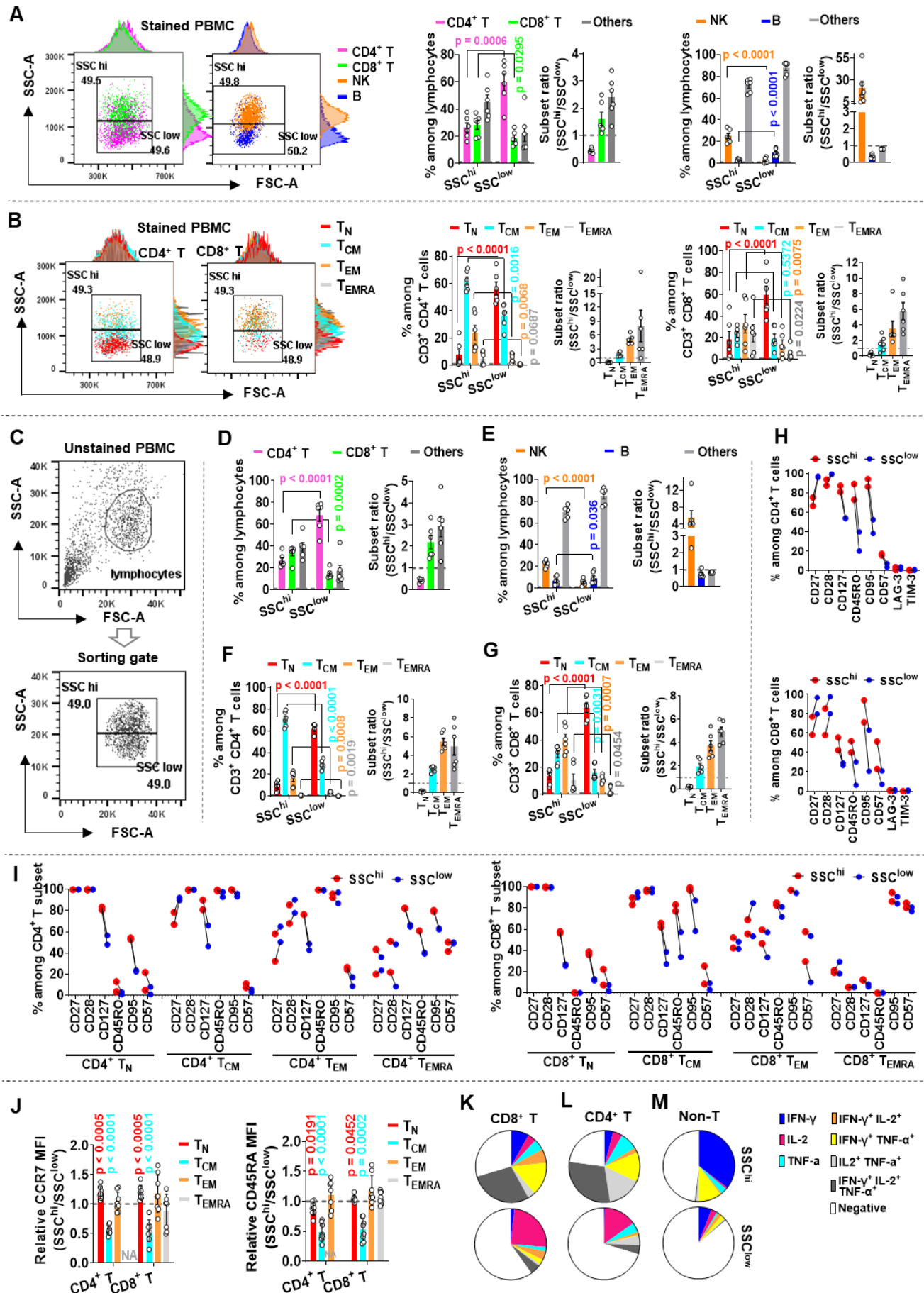260   (main text continued after Figure 2)

261

262 **Figure 2. SSC is a robust biophysical property for TRuST development**

263 (**A and B**) PBMC samples were stained with surface marker antibodies before flow cytometry

264 data acquiring. Dot plots are representative FSC/SSC profiles of CD3$^+$ CD4$^+$ T/CD3$^+$ CD8$^+$ T

265 cells (**A, left dot plot**), NK/B cells (**A, right dot plot**), and T$_N$/T$_{CM}$/T$_{EM}$/T$_{EMRA}$ cell subsets (**B**).

266 For statistical analysis, samples were gated to equally divide the cells into two clusters based

267 on the cluster of total lymphocytes (not shown in the dot plots) (**A and B, dot plots**) and the

268 percentage of CD3$^+$ CD4$^+$ T/CD3$^+$ CD8$^+$ T cells, NK/B cells, and T$_N$/T$_{CM}$/T$_{EM}$/T$_{EMRA}$ cell subsets

269 within SSC^{hi} or SSC^{low} cluster were summarized (**A and B, histograms**). Two independent

270 experiments for each donor (n = 3) were compiled. A two-tailed, paired *t*-test between the two

271 groups was performed. Error bars indicate mean ± SEM.

272 (**C-G**) Unstained PBMC samples were equally sorted into SSC^{hi} and SSC^{low} populations before

273 lymphocyte subtypes determination (**C**). Characterization of the percentage of CD3$^+$ CD4$^+$

274 T/CD3$^+$ CD8$^+$ T cells (**D**), NK/B cells (**E**), and T$_N$/T$_{CM}$/T$_{EM}$/T$_{EMRA}$ (**F and G**) among the sorted

275 SSC^{hi} and SSC^{low} cell populations. Data from three donor samples with two independent

276 experiments for each donor were compiled. A two-tailed, paired *t*-test between the two groups

277 was performed. Error bars indicate mean ± SEM.

278 (**H and I**) A comparison of the expression profiles of selected phenotyping markers in sorted

279 SSC^{hi} and SSC^{low} cells (**H**), and characterization of the phenotypic traits of the same

280 naïve/memory T subset derived from SSC^{hi} or SSC^{low} cell clusters (**I**). Each dot represents data

281 of one donor PBMC (**H and I**).

282 (**J**) The relative expression level of CCR7 and CD45RA in CD4$^+$ T or CD8$^+$ T naïve/memory

283 subsets from sorted SSC^{hi} and SSC^{low} cells. Plots represent data from three donor PBMC. Cell

15

284   subset nearly undetectable is indicated as "NA". A two-tailed, unpaired t-test between SSC^{hi}

285   and SSC^{low} groups was performed. Error bars indicate mean ± SEM.

286   (**K-M**) Sorted SSC^{hi} and SSC^{low} cells were stimulated with PMA plus ionomycin for 4 hours

287   before intracellular staining. Shown are the multifunctional cytokine expression profile of CD3^{+}

288   CD8^{+} T cells (**K**), CD3^{+} CD8^{-} T cells (**L**), and CD3^{-} cells (**M**) within sorted sorted SSC^{hi} or SSC^{low}

289   cells (n = 2).

290   See also **Figure S1** for gating methods in determining cell types and multifunctionality analysis,

291   **Figures S2** and **S3** for manual gating selection.

292

293   **TRuST enhances lymphocyte subset selection using computational gate design**

294   While manual gating for cell sorting is a simple and effective way to reconstitute

295   lymphocytes, it could be less efficient for the selection of specific lymphocyte subset.

296   Thus, we took advantage of the recently developed computational algorithm, GateID

297   (Baron et al., 2019), that relies on the general properties (e.g. cell size, granularity and

298   mitochondrial content) to search for the optimum gate for cell type enrichment. Using

299   this method, it is possible to obtain lymphocyte subsets of interest with desired purity

300   and yield (**Figure 3**).

301

302   Naïve T cells can be obtained with the highest purity and acceptable yield (**Figure 3E**),

303   in line with their location within the cell group of lowest SSC (**Figure 2B**). T$_{CM}$, T$_{EM}$,

304   T$_{EMRA}$, total CD4^{+} T and NK cells can also be significantly enriched, but at the expense

305   of quickly dropped yields (**Figures 3F-3H, 3A, and 3C**). On the other hand, CD8^{+} T

306   cells and B cells tend to be the most difficult lymphocytes to be enriched with an

307   improved purify and appreciable yield, partially due to their relatively homogeneous

308   side-scattering distribution diffused into other lymphocytes (**Figures 3B and 3D**).

309   Notably, given that a comparable FSC/SSC pattern was observed between unstained

310   and stained cell samples (**Figure S3B**), it would be possible to directly apply the

311   predicted gate in actual sorting experiments without gate normalization. Thus,

312   combining TRuST with computational gate search, it is feasible to improve the purity

313   of lymphocyte subsets with a reduced yet still acceptable recovery rate.

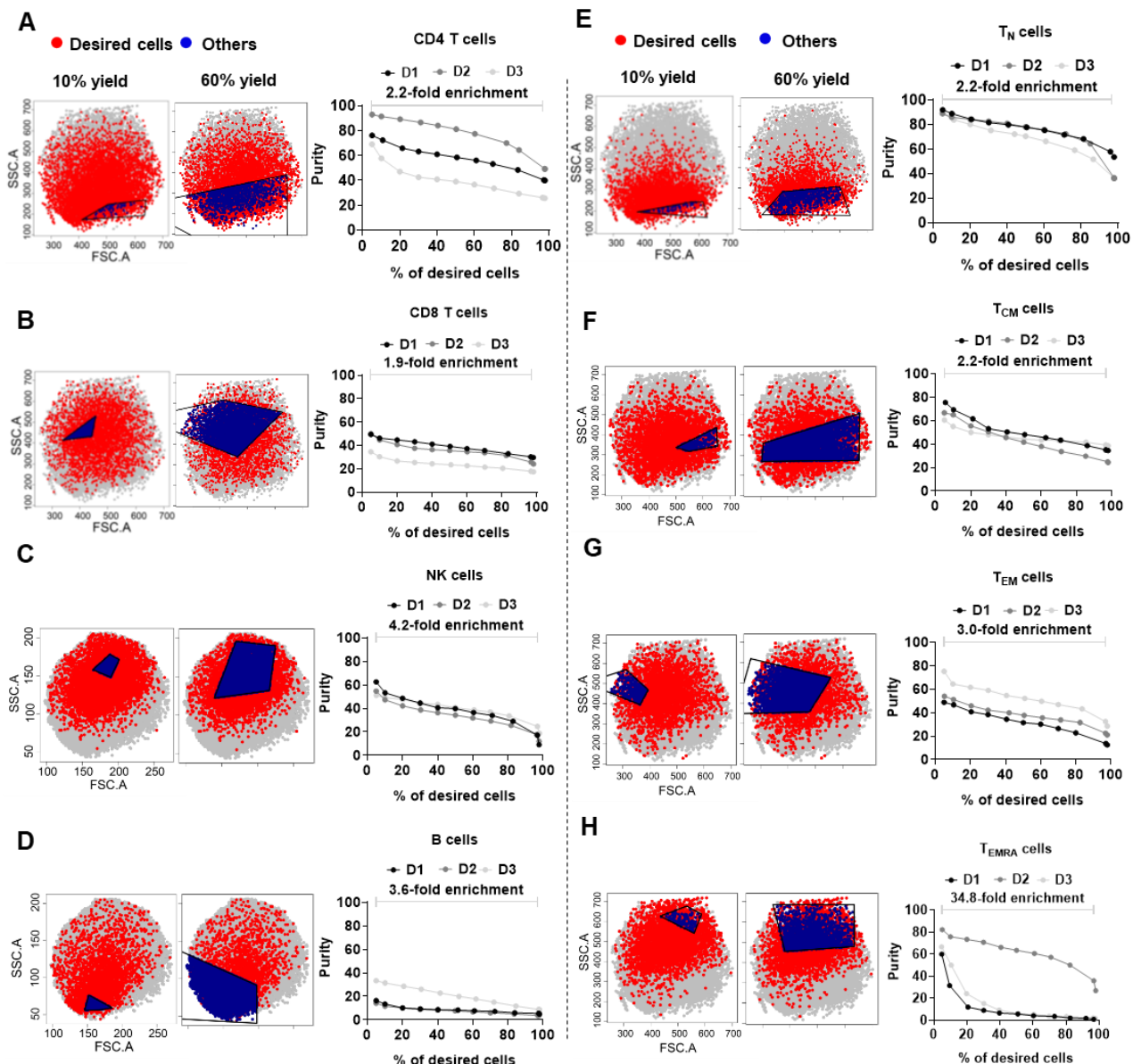314   (main text continued after Figure 3)

17

Figure 3. TRuST enhances enrichment of specific lymphocyte subset using computational gate design

(**A-H**) The raw readouts corresponding to FSC and SSC parameters for each cell type as shown in Figures 2A and 2B were exported, named and reanalyzed by GateID algorithm to select the desired cell type. The enrichment efficiency of CD3$^+$ CD4$^+$ T (**A**), CD3$^+$ CD8$^+$ T (**B**), NK (**C**) and B cells (**D**), or selection of total T$_N$ (**E**), T$_{CM}$ (**F**), T$_{EM}$ (**G**) and T$_{EMRA}$ subsets (**H**) were plotted by automatically adjustable gating threshold. For each cell type/subset, two representative gating plots corresponding to 10% and 60% yields of desired cells, and the correlation plots between

323   purity and yield are shown. An average enrichment fold-increase between ~100% yield to ~5%

324   yield (n = 3) is indicated. The percentage of desired cells (yield) is calculated as the number of

325   desired cells within the gating to that of total desired cells among the whole cell population. The

326   purity indicates the proportion of desired cells to that of total cell numbers within each gate.

327   See also **Methods**.

328

329   **TRuST-relied lymphocytes reconstitution improves T cell product quantity and**

330   **quality**

331   When practical feasibility and manufacturing cost are taken into consideration, such

332   as T cell production for adoptive immunotherapy, it might not be necessary to enrich

333   for a very specific cell type at the expense of greatly reduced cell recovery. Instead,

334   strategies that enable the reconstitution of lymphocyte subpopulations to maximally

335   improve cell production without compromising yield and quality would be preferable.

336

337   Given that T cell product derived from less-differentiated T cells show better outcome

338   in adoptive immunotherapy (Berger et al., 2008; Finney et al., 2019; Fraietta et al.,

339   2018; Hinrichs et al., 2011), we next investigated how compositional difference of

340   starting T cell materials reconstituted solely by TRuST under manual gate selection

341   (**Figure 2C**) may affect the diversity of final T cell products. In response to anti-

342   CD3/CD28 microbeads stimulation, an antigen-presenting cells-mimic activation

343   approach widely used for T cell manufacturing, SSC^{low} cells consisting of T_N and

344   younger T_{CM} cells were endowed with superior proliferation capacity, and achieved an

19

345   average increase of total nucleated cells (TNC) by 2.3-fold at day 7 and 3.2-fold at day

346   11 with 3-fold increase for CD4$^+$ T and 4-fold increase for CD8$^+$ T subtypes (**Figures**

347   **4A-4C and S4A-S4C**). Unexpectedly, the expansion potential of the SSC$^{high+low}$ group

348   appeared to be equivalent to that of SSC^{high} population (**Figures 4A-4C**), likely due to

349   the precocious differentiation of naïve cells driven by existing effector/memory cells

350   (Klebanoff et al., 2016) and the inhibitory effects caused by large amount of NK cells

351   (Cook and Whitmire, 2013).

352

353   Yellow fever-specific central memory CD8$^+$ T cells with high CD45RA expression was

354   demonstrated to be a critical cell subpopulation accounting for persistent immune

355   memory, which resembled stem cell-like memory subset (CCR7$^+$ CD45RA$^+$ CD58$^+$

356   CD95$^+$ CD28$^+$ CD27$^+$ T$_{SCM}$) (Fuertes Marraco et al., 2015). Thus, based on the dynamic

357   change of CCR7/CD45RA expression, an in-depth gating strategy was used to classify

358   T cell subsets into T$_N$, naïve population-closest CD45RA^{high} T$_{CM}$ (T$_{CMRA-hi}$), CD45RA^{low}

359   T$_{CM}$ (T$_{CMRA-low}$), CD45RA^{negative} T$_{CM}$ (T$_{CMO}$), and T$_{EM}$ with CD45RA expression as

360   CD45RA^{high} T$_{EM}$ (T$_{EMRA-hi}$), CD45RA^{low} T$_{EM}$ (T$_{EMRA-low}$) and CD45RA^{negative} T$_{EM}$ (T$_{EM}$)

361   (**Figure S4D**). Longitudinal assessment of T cell naïve/memory composition during

362   expansion showed that, compared to SSC^{high} descendants, SSC^{low} cells-derived

363   progenies generally had a higher portion of T$_{CMRA-hi}$ but less T$_{CMRA-low}$ and other more-

364   differentiated cell subsets (e.g. T$_{CMO}$ and T$_{EMRA-low}$) (**Figures 4D, 4E, and S4E-S4H**).

365   This finding is consistent with a continuously higher expression of co-stimulatory

366   molecules CD27/CD28 that favor cell survival and proliferation (**Figures 4F, S5A, and**

20

367 **S5B**) while other phenotypic traits like memory marker CD45RO and

368 inhibition/senescence receptors such as CD57, LAG-3 and TIM-3 were more

369 dynamically variable (**Figures S5A and S5B**).

370

371 Functionally, the SSC^{low} cells-derived products responded faster to short period of PKC

372 activation by producing more IL-2 and TNF-α but less IFN-γ (**Figure 4G**). SSC^{low} cells-

373 derived CD4$^+$ T cells displayed better compliance with this tendency by expressing the

374 highest amount of early-effector cytokines (e.g. IL-2$^+$ and IL-2$^+$ TNF-α$^+$) and less late-

375 effector cytokines (e.g. IFN-γ$^+$, IFN-γ$^+$ IL-2$^+$ and IFN-γ$^+$ TNF-α$^+$) (**Figure 4H**). The CD8$^+$

376 T counterpart shows a higher diversity and even conflicts these observations post

377 extensive expansion (e.g. donor 3 at day 11) (**Figure 4I**). Nevertheless, the global

378 cytokine-expressing trait of cell products generated from SSC^{low} group is more naïve-

379 like (**Figures S5C and S5D**) (Gattinoni et al., 2005; Hinrichs et al., 2009), indicating a

380 synergic functionality may happen when CD4$^+$ T and CD8$^+$ T co-exist in culture system.

381 Superior engraftment and persistence of infused T cells are critical parameters for

382 improved therapeutic index. Extensively expanded T cells from either SSC^{high}, SSC^{low}

383 or reconstituted SSC$^{high+low}$ group had similar chemotactic migration to CCL19/CCL21

384 (**Figure 4J**), in line with their comparable proportion of total T$_{CM}$ (**Figures 4D and 4E**).

385 However, in response to multiple stimulation by CD3/CD28 engagement, the SSC^{low}-

386 derived progenies were endowed with greater capability for multiple expansion under

387 both IL-2 and homeostatic cytokines IL-7/IL-15 (**Figure 4K**), presumably associated

388 with a higher expression of costimulatory markers CD27/CD28 (**Figures 4F, S5A, and**

389   **S5B**) and underlined epidemic modification favoring cell persistence.

390

391   Overall, the SSC^{low} lymphocytes-derived T cell product is discernable from that of

392   SSC^{high} group, the former manifests not only superior proliferation but also earlier

393   phenotypes characteristic of apparently increased T$_{CMRA-hi}$ and enhanced IL-2/TNF-α

394   expression for both CD4$^+$ T and CD8$^+$ T cells ((**Figures 4L and 4M**).
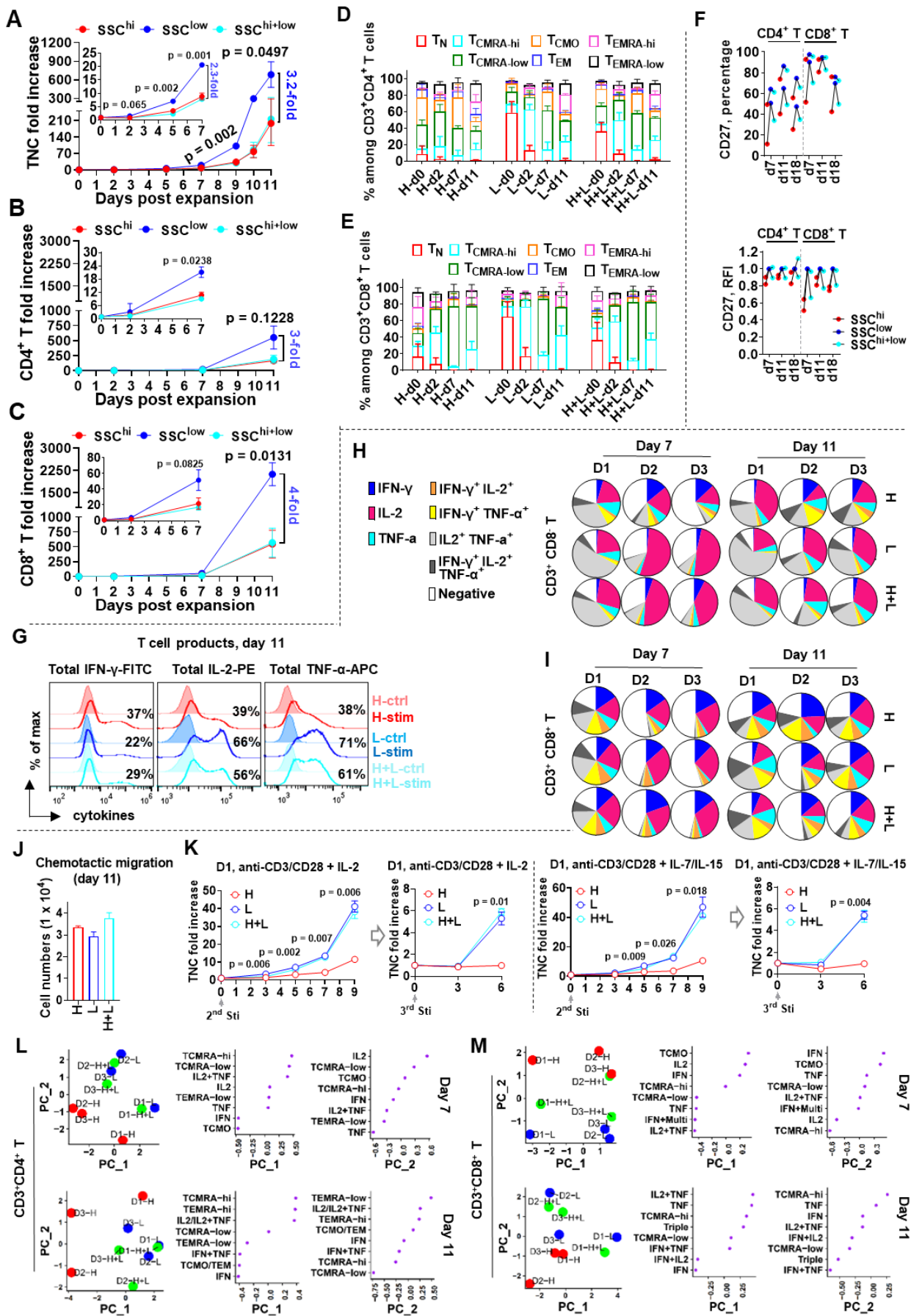
395   (main text continued after Figure 4)

23

397 **Figure 4. TRuST-relied lymphocytes reconstitution improves T cell product quantity and**

398 **quality**

399 (**A-C**) Expansion efficiency of lymphocytes derived from SSC^{hi}, SSC^{low}, or reconstituted

400 SSC^{hi+low} cells at a ratio of 1:1 are represented by TNC fold increase (**A**), CD3$^+$ CD4$^+$ T (**B**) and

401 CD3$^+$ CD8$^+$ T fold increase (**C**). Data are presented as means ± S.E.M (n = 3). Paired two-tailed

402 *t*-test between SSC^{low} and SSC^{hi} group was performed. Error bars indicate mean ± SEM.

403 (**D and E**) Compositional change of naive/memory subsets in CD3$^+$ CD4$^+$ T (**D**) or CD3$^+$ CD8$^+$

404 T cells (**E**) plotted along the days of expansion. Error bars indicate mean ± SEM.

405 (**F**) Percentage and relative fluorescence intensity (RFI) of CD27.

406 (**G-I**) Representative histogram plot of IFN-γ/IL-2/TNF-α expression of cell product at day 11

407 post expansion derived from cell groups with different side-scattering intensity (**G**).

408 Multifunctional cytokine expression of total CD4$^+$ T (**H**) or CD8$^+$ T (**I**) cells at day 7 and day 11

409 post expansion (n = 3) with 2 independent experiments for donor 1 and 2.

410 (**J**) Migration capacity of T cells at day 11 post expansion derived from SSC^{hi}, SSC^{low} and

411 SSC^{hi+low} groups. Error bars indicate mean ± SEM.

412 (**K**) Responsiveness of effector cells descended from SSC^{hi}, SSC^{low} and SSC^{hi+low} groups at

413 day 11 post expansion to multi-stimulation by CD3/CD28 engagement with IL-2 (**top**) or

414 homeostatic cytokines IL-7 plus IL-15 (**bottom**). Duplicates for each sample were performed.

415 Unpaired two-tailed *t*-test between SSC^{low} and SSC^{hi} group was performed. Error bars indicate

416 mean ± SEM.

417 (**L and M**) All phenotypic parameters and cytokine-expressing values were integrated together

418 for PCA calculation. For data from day 7, IFN-γ$^+$ IL-2$^+$/ IFN-γ$^+$ TNF-α$^+$/ IFN-γ$^+$ IL-2$^+$ TNF-α$^+$ were

419   combined as "IFN+Multi". "H" and "L" indicate "SSC^{hi}" and "SSC^{low}", respectively.

420   See also **Figures S4A-4C and S4E-4G** for individual data, and **Figure S4D** for gating method

421   in cell differential lineages characterization.

422

423   **Increased $T_{CMRA\text{-}hi}$ derived from the SSC^{low} cell cluster resembles central memory**

424   **precursors**

425   Given the significant accumulation of $T_{CMRA\text{-}hi}$ subpopulation that falls in the

426   conventional central memory gate of the cell products derived from SSC^{low} group

427   (**Figures S4D and S1B**), we next sought to define the natural characteristics of this T

428   cell subset by longitudinally determining its phenotypic change during expansion

429   (**Figures 5A-5E**). We showed that $T_{CMRA\text{-}hi}$ had a higher expression of canonical

430   memory marker CD45RO than T_N but lower than $T_{CMRA\text{-}low}$ and T_{CMO} regardless of $CD3^+$

431     $CD4^+$ T cells (**Figures 5B and 5C**) or $CD3^+$ $CD8^+$ T cells (**Figures 5D and 5E**). While

432   all resting central memory T subsets ($T_{CMRA\text{-}hi}$, $T_{CMRA\text{-}low}$ and T_{CMO} at day 0) presented

433   higher death receptor CD95 (a marker used to distinguish T_{SCM} from T_N) (Fuertes

434   Marraco et al., 2015; Gattinoni et al., 2011) than the T_N subset, they became similar

435   post activation with nearly complete expression of this marker (**Figures 5B-5E**).

436   Notably, the expression of co-stimulatory markers such as CD27 and CD28 was more

437   comparable between $T_{CMRA\text{-}hi}$ and T_N, especially for $CD8^+$ T cells (**Figures 5D and 5E**).

438   With regard to inhibitory or senescent factors (e.g. CD57, LAG-3 and TIM-3), $CD8^+$

439     $T_{CMRA\text{-}hi}$ and $CD8^+$ T_N expressed similar but less CD57 than other $CD8^+$ T subsets

440   before activation, which however decayed to a dim expression in all subsets post

441 extensive proliferation (**Figure 5D**). In addition, LAG-3 was dramatically increased in

442 activated CD8$^+$ T subsets at day 7 and decreased at day 11, during which $T_{CMRA-hi}$

443 tended to have a higher LAG-3 expression compared to T_N but still comparable or even

444 lower than other memory subsets (**Figures 5D and 5E**). These findings suggest that

445 $T_{CMRA-hi}$ is phenotypically distinct from T_N and resembles the central memory precursor

446 with naïve-like phenotypic traits (CCR7$^+$ CD45RA^{high} CD95$^+$ CD28$^+$ CD27$^+$), which

447 could be taken into consideration in the evaluation of T cell products by different

448 manufacturing protocols.

449

450 The burst increase of $T_{CMRA-hi}$ at the beginning of T cell activation (day 2, **Figures 4D**

451 **and 4E**) is well correlated with the initial proportion of T_N, and this trend maintains from

452 day 7 to day 11 (**Figure 5F**). In contrast, the existence of more-differentiated CD4$^+$

453 T_{CMO} (**Figure 5G**) and CD4$^+$ $T_{CMRA-low}$ (**Figure 5H**) in starting cell materials tend to

454 counteract the generation of CD4$^+$ $T_{CMRA-hi}$ despite the effects being varied at different

455 stages post activation. Also, a high number of CD8$^+$ $T_{CMRA-low}$ (**Figure 5H**) and CD8$^+$

456 T_{EMRA} (**Figure 5I**) are more likely to reduce the production of CD8$^+$ $T_{CMRA-hi}$. However, it

457 is less predictable for CD8$^+$ $T_{EMRA-hi}$ generation based on the cell composition before

458 expansion (**Figures S6D-S6G**). Of note, CD4$^+$ T_N and CD4$^+$ T_{CMO} (**Figures S6D and**

459 **S6E**) do show evidences of contrary correlation with CD4$^+$ $T_{EMRA-hi}$ production. There

460 was a sharp decrease of CD8$^+$ $T_{EMRA-hi}$ cells post activation in the SSC^{high} group that

461 consists of a larger proportion of differentiated cell subpopulations (**Figures S4E and**

462 **S4F**). Thus the dynamical accumulation of terminally differentiated $T_{EMRA-hi}$ cells from

463   SSC^{low} groups (**Figures S4F and S4G**) could be partially attributed to a more survival-

464   favoring environment enriched in less-differentiated cell subsets (e.g. T_N). Additionally,

465    $T_{EMRA-hi}$ displays higher CD27/CD28 expression than the CD45RA-reduced $T_{EMRA-low}$ or

466   T_{EM} subset, which is especially apparent for CD8$^+$ T cells during expansion (**Figures**

467   **5D and 5E**), suggesting functional potency of this cell subset in cell therapy when

468   alternative co-stimulatory signaling (e.g. CD28 and 4-1-BB) and accessory factors for

469   end-stage effector cells proliferation are involved (Fuertes Marraco et al., 2015; van

470   Leeuwen et al., 2002; Waller et al., 2007). Taken together, these results show that the

471   pre-enrichment of less-differentiated cells simply by side scatter enables the

472   maintenance of naïve-like central memory precursors ($T_{CMRA-hi}$) and accordingly

473   contributes to the slight accumulation of terminally effector-like T_{EM} ($T_{EMRA-hi}$).

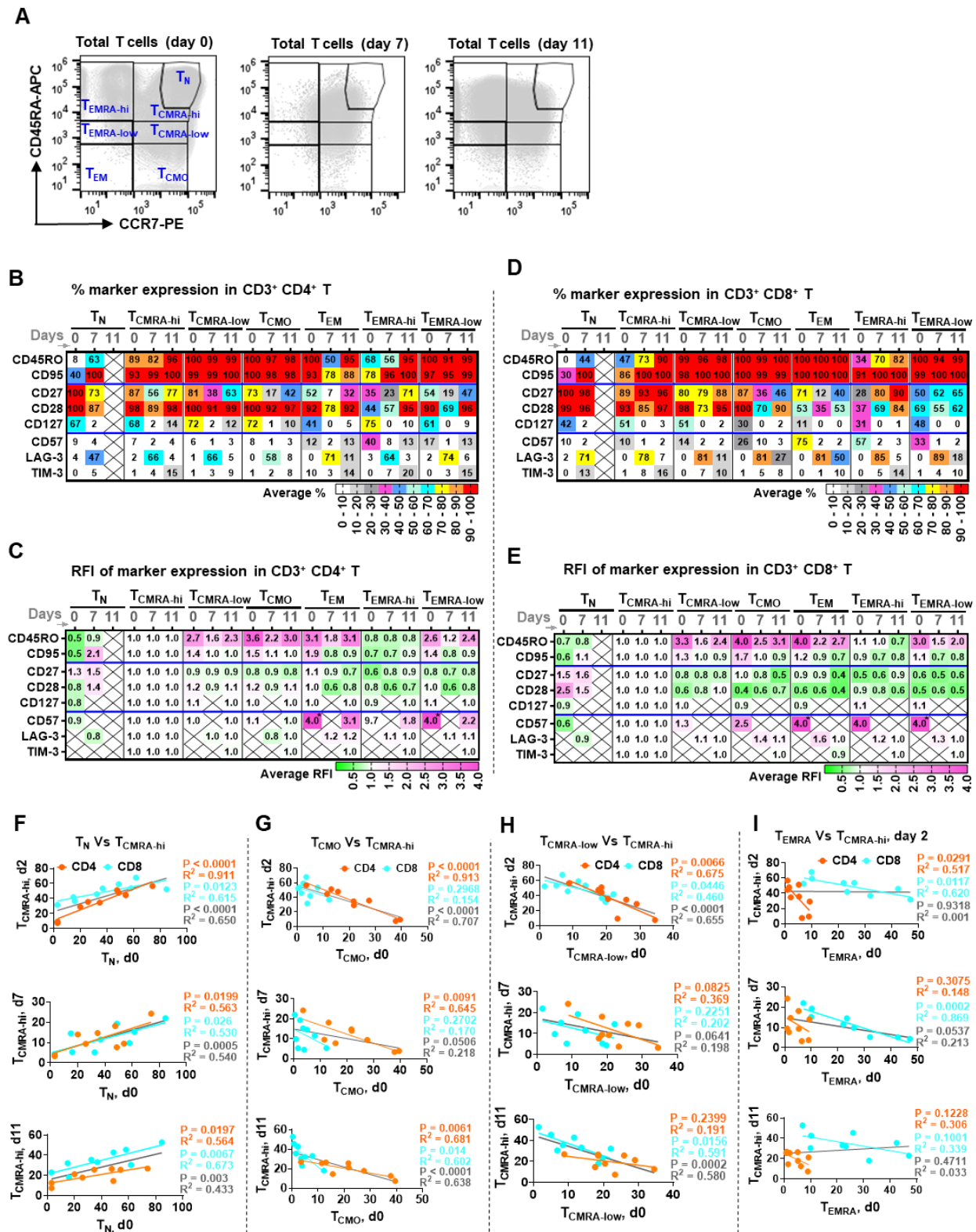474   (main text continued after Figure 5)

27

Figure 5. Increased $T_{CMRA-hi}$ derived from SSC^{low} cell cluster resembles central memory precursor

(**A**) Representative plots show the superimposed total T cell populations derived from SSC^{hi},

28

478   SSC^{low} and SSC^{hi+low} cells at day 0, 7, 11. T cell subsets to be analyzed are gated.

479   (**B-E**) Longitudinal assessment of phenotypic change of T$_{CMRA-hi}$ compared to other T cell

480   subsets. Average expression frequency of the indicated markers within CD4$^+$ T or CD8$^+$ T

481   subsets (**B and E**) and abundance as presented by relative fluorescence intensity (RFI) was

482   reported after normalization to the values of T$_{CMRA-hi}$ for each marker of the same time points

483   respectively (**C and E**). The numbers highlighted by "*" indicate values large than 4. The cross

484   indicates omitted data due to low cell percentages for marker expression identification or

485   insufficient counts for MFI calculation.

486   (**F-I**) Correlation analysis of starting effector/memory composition, including T$_N$ (**F**), T$_{CMO}$ (**G**),

487   T$_{CMRA-low}$ (**H**), and total T$_{EMRA}$ (**I**), with the percentage of generated T$_{CMRA-hi}$ among cell products

488   of each time point. Data from the same day from all of the three donors were combined. Each

489   dot represents the percentage of generated T$_{CMRA-hi}$ versus the initial cellular component of its

490   starting cell material (day 0). The solid black line indicates combined linear regression using all

491   the dots in that plot (**F-I**).

492   See also **Figure S4D** for gating method in identifying the dynamic change of T cell lineages

493   during expansion, and **Figures S6A-6C** for individual data of phenotypic marker expression in

494   each T cell subset. **Figures S6D-6G** for correlation analysis of initial cell composition with T$_{EMRA-}$

495    $_{hi}$ generation.

496

497   **CD4$^+$ T cells help is critical for optimum CD8$^+$ T cells proliferation**

498   A shaper ratio decrease of CD4/CD8 T cells during expansion was observed for cells

499   from lower side-scatter, which initially have the largest proportion of CD4$^+$ T cells and

500   later the highest expansion capacity (**Figure 6A**). This has inspired us to understand

501   the role of CD4$^+$ T-CD8$^+$ T cells crosstalk in T cell proliferation and functionality shaping

502   despite the absence of specific external antigens (**Figure 6B**).

503

504   Co-culture of CD4$^+$ T-CD8$^+$ T cells favored the global expansion of total T cells (**Figure**

505   **6C**). Help from CD4$^+$ T cells was required for CD8$^+$ T cells maximal proliferation by an

506   average of 6-fold increase at day 7 and 8.5-fold increase at 18 (**Figure 6D**). In turn,

507   CD8$^+$ T cells reduced CD4$^+$ T cells expansion to a lesser extent by 1.4-fold reduction

508   at day 7 and 2-fold decrease at day 11 and 18 (**Figure 6E**). Thus, the orchestrated

509   growth dynamics within CD4$^+$ T and CD8$^+$ T cells results in final T cell products with

510   not only different absolute cell numbers (**Figure 6C**) but also discernable CD4$^+$ T to

511   CD8$^+$ T ratio (**Figure 6F**).
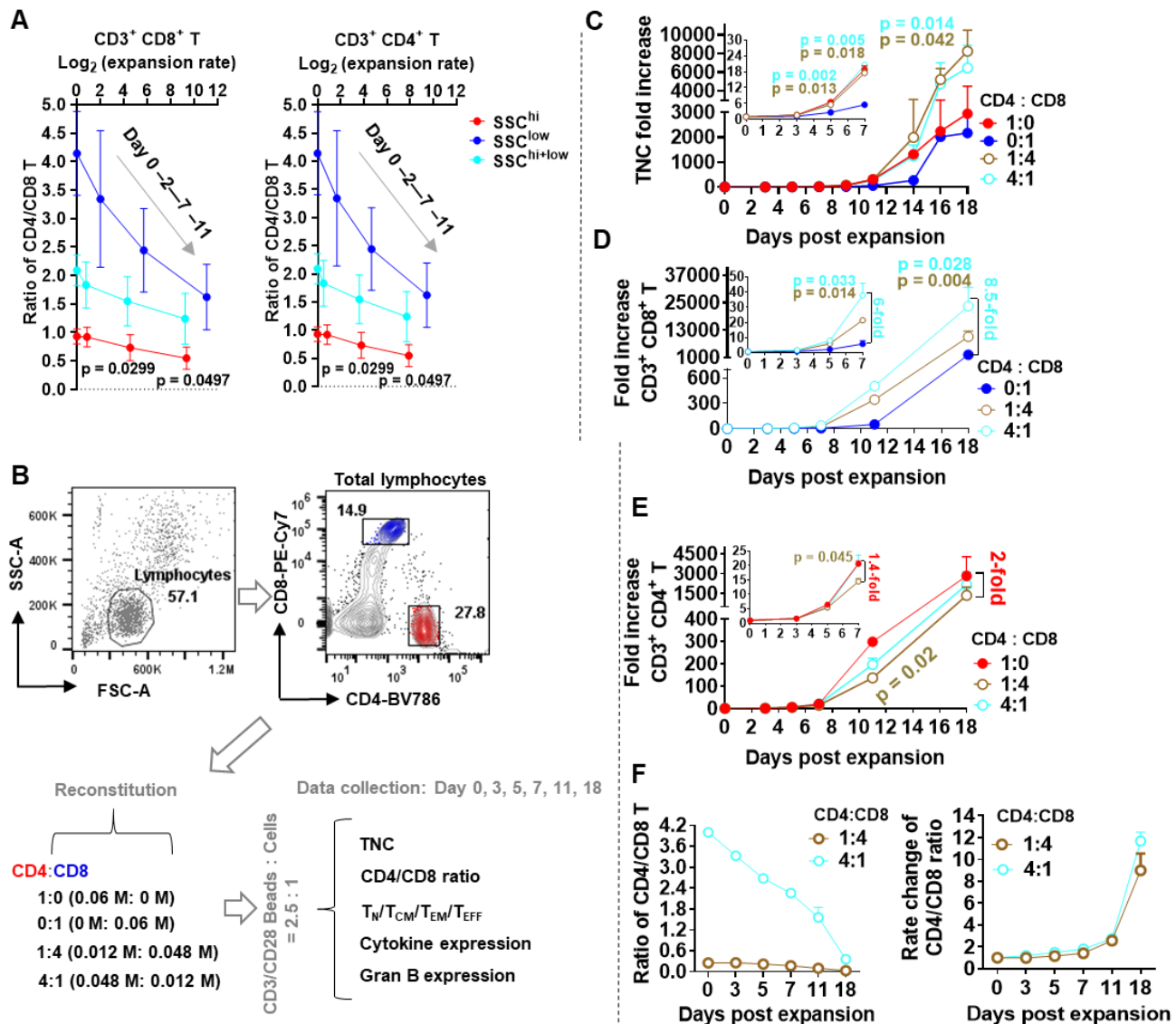
512   (main text continued after Figure 6)

Figure 6. CD4+ T help is required for optimal CD8+ T expansion

(**A**) Synchronized T cell expansion efficiency with the ratio change of CD4/CD8 T cells starting

from cell materials of different side-scattering intensity. Data are representative of three donors

as described in Figures 4A-4C. Graphs represent means ± S.E.M (n = 3). Paired two-tailed *t*-

test was used for statistical calculation between SSC^{hi} and SSC^{low} group. Error bars indicate

mean ± SEM.

(**B**) CD4+ cells and CD8+ cells were sorted and validated to have more than 96% of CD3+ CD4+

T and CD3+ CD8+ T cells, respectively. CD4+ cells and CD8+ cells were reconstituted at the

521   indicated ratio and co-expanded by CD3/CD28 engagement.

522   (**C-E**) Proliferative potential of TNC (**C**), CD3$^+$ CD4$^+$ T (**D**) or CD3$^+$ CD8$^+$ T cells (**E**) in condition

523   of CD4-CD8 T cells co-culture. Data of day 5, 7, 11 and 18 represent two independent

524   experiments. Unpaired two-tailed *t*-test compared to culture condition of CD8$^+$ T cells only (**C**

525   **and D**) or CD4$^+$ T cells only (**E**). Error bars indicate mean ± SEM.

526   (**F**) Changes in the ratios of CD4$^+$ T to CD8$^+$ T cells in samples starting with high (4:1) and low

527   (1:4) ratios of CD4 to CD8 T cells. Error bars indicate mean ± SEM.

528

529   **CD4$^+$ T cells promote CD8$^+$ T early central memory pool maintenance**

530   By longitudinal assessment of T cell naive/memory composition, we found that

531   optimum maintenance of CD8$^+$ T$_{CMRA-hi}$ but less CD8$^+$ T$_{EM}$ and CD8$^+$ T$_{EMRA-low}$ can be

532   achieved in the presence of CD4$^+$ T cells in a ratio-dependent manner (**Figure 7A**).

533   Interestingly, the mild accumulation of CD8$^+$ T$_{EMRA-hi}$ was also observed, similar to that

534   of SSC^{low} cells-derived descendants (**Figures S4F and S4G**), indicating a superior

535   culture environment for T cell survival endowed by CD4$^+$ T. On the contrary, a large

536   proportion of CD8$^+$ T cells tended to counteract CD4$^+$ T$_{CMRA-hi}$ generation during the

537   early expansion stages (e.g. day 0-7) (**Figure 7B**). This is reflected by a higher

538   expression of CD28 on CD8$^+$ T cells but lower on CD4$^+$ T cells throughout the co-

539   culture course (**Figures 7C**, **S7A, and S7B**). Also, the increased number of less-

540   differentiated CD8$^+$ T cells generated at day 11 under CD4$^+$ T-CD8$^+$ T co-expansion is

541   consistent with a greater migration ability to CCL19/CCL21 (**Figure 7D**).

542

543 With respect to functional shaping, it is clear that CD4$^+$ T and CD8$^+$ T cells mutually

544 endowed each other with a higher granzyme B expression during the initial proliferation

545 phase (day 0 - 7, **Figures 7E and 7F**). However, CD8$^+$ T cells from all conditional

546 groups became comparable in granzyme B expression at day 11 while a larger portion

547 of CD4$^+$ T cells continued to express granzyme B in the presence of CD8$^+$ T cells

548 (**Figures 7F**). In addition, CD4$^+$ T help contributed to the generation of less-

549 differentiated CD8$^+$ T cells characteristic of enhanced IL-2 /TNF-α but reduced IFN-γ

550 production (**Figures 7G**). Instead, CD8$^+$ T cells showed only moderate inhibition on

551 the secretion of IL-2/TNF-α by CD4$^+$ T cells (**Figures 7G**). Moreover, the inclusion of

552 resting CD4$^+$ T cells was able to rescue the expansion potency of extensively

553 differentiated CD8$^+$ T cells (**Figures 7H**). Therefore, despite the absence of cognate

554 antigens, help from CD4$^+$ T cells is critical for shaping the proliferative capacity and

555 functional potency of CD8$^+$ T cells, which should be an important factor to be

556 considered during T cell manufacturing.
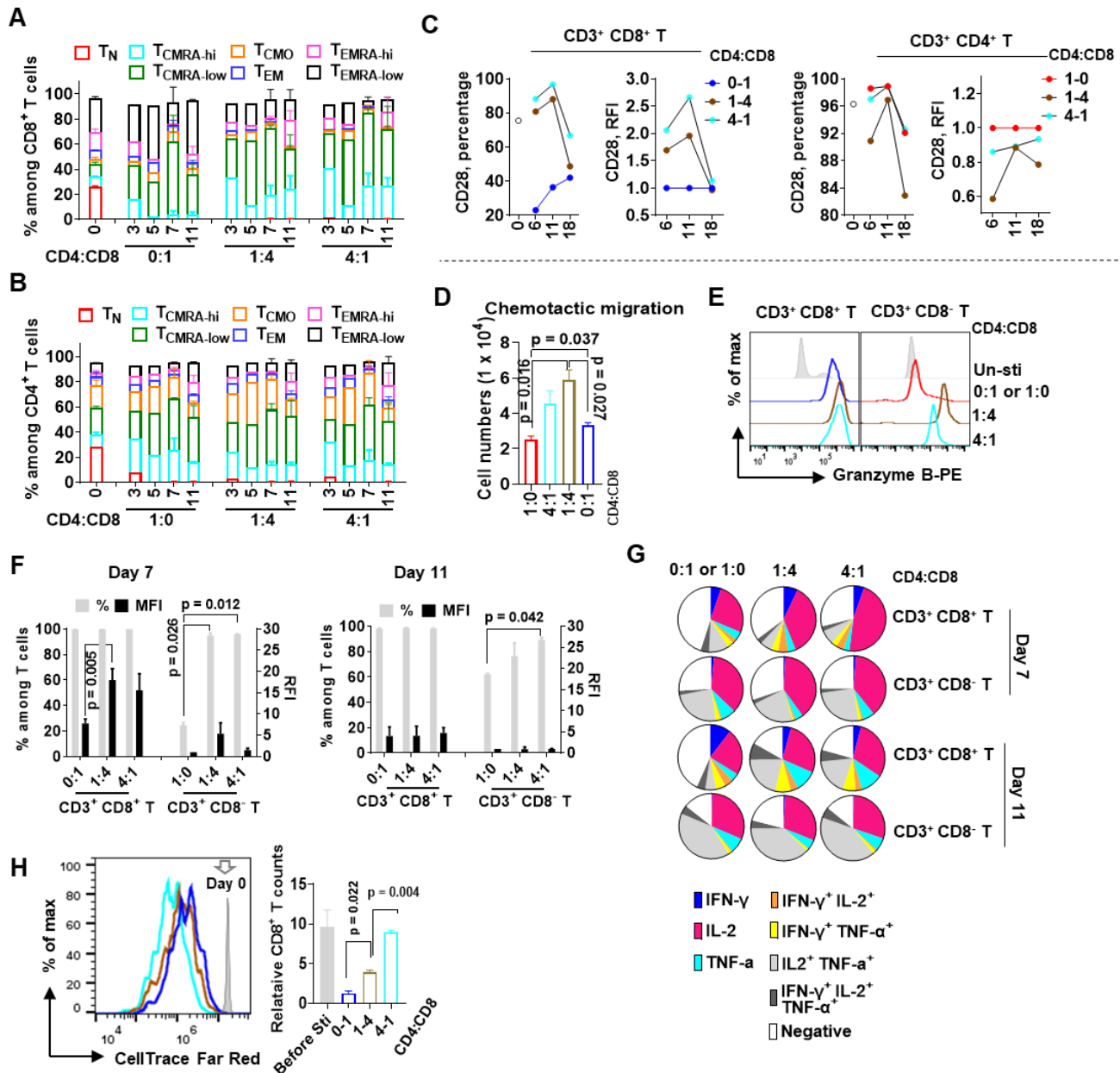
557 (main text continued after Figure 7)

33

Figure 7. CD4+ T cells promote the maintenance of CD8+ T early central memory pool

(**A and B**) Compositional change of naive/memory subsets in CD3+ CD8+ T (**A**) or CD3+ CD4+

T cells (**B**) along the days of expansion. Data for day 0, 7 and 11 are representative of two

independent experiments. Error bars indicate mean ± SEM.

(**C**) Dynamic expression of CD28 is represented by both percentage and relative fluorescence

intensity of T cell products from CD4-CD8 T cells co-expansion. The medium fluorescence

intensity (MFI) is normalized to that of CD4+ T cells or CD8+ T cells cultured separately at the

34

565   indicated time points.

566   (D) CCL21/CCL19-driven migration capacity of T cell generated at day 11 starting from different

567   CD4$^+$ to CD8$^+$ T cell ratio. Data represents duplicate experiments. Error bars indicate mean ±

568   SEM.

569   (E and F) Representative plot of granzyme B-expressing T cells at day 7 post expansion (E)

570   and summary of T cells in granzyme B expression from data of two independent experiments

571   (F). Error bars indicate mean ± SEM.

572   (G) Multifunctional cytokine expression of CD3$^+$ CD8$^+$ T or CD3$^+$ CD4$^+$ T cells at day 7 and day

573   11 post expansion.

574   (H) Resting CD4$^+$ T cells were sorted and spiked into CellTrace dye-labeled T cell products (day

575   13) at the indicated ratio and co-stimulated (cells to beads = 1 : 1) for 4 days. Duplicates for

576   each group were performed. Cells were counted at day 4 before collection for anti-CD4-BV786

577   staining and analysis by flow cytometer. Cell counts were normalized to cell group without newly

578   added CD4$^+$ T. Unpaired two-tailed t-test between two groups was performed. Error bars

579   indicate mean ± SEM.

580   See also **Figure S7**.

581

582   **DISCUSSION**

583   TRuST provides a novel method that enables label-free reconstitution of lymphocyte

584   subpopulations using the intrinsic side-scattering property of cells. We demonstrate

585   that less-differentiated T cells are endowed with a lower SSC intensity, which, together

586   with a high ratio of CD4/CD8 T cells, can be effectively enriched and used for optimum

587   T cell production (**Figures 2 and 4**). Furthermore, we address that both naïve T cells

588   and a higher $CD4^+$ T to $CD8^+$ T proportion are critical for maximal $CD8^+$ T cells

589   expansion and optimal $CD8^+$ T memory precursors maintenance (**Figures 5-7**).

590

591   Naïve T cells have discernable morphological profiles from memory/effector T cells

592   under transmission electron microscope (Dimeloe et al., 2016). Our work

593   demonstrates that this difference can be recaptured simply by using the side-scattering

594   property, which would be more practically meaningful in a high-throughput and cost-

595   effective manner. We showed that SSC is a robust biophysical attribute, the distribution

596   pattern of which presents the intrinsic granularity difference of cellular context and is

597   unaffected by either sample processing or voltage changes applied during data

598   acquisition (**Figures S3A-S3D**). Thus, when applying the gate settings determined

599   using pre-stained cell samples to the unstained cell samples, no gating normalization

600   is required for T cell reconstitution by manual gate selection (**Figures 2 and 4)** and

601   only slight gating correction is required for cell type purification by computational gate

602   search (**Figure 3**). With a single sorting step based on the SSC intensity, lymphocyte

603   populations with high $CD4^+$ T to $CD8^+$ T ratio are clustered together with younger T

604   cells (e.g. T_N and early T_{CM}) among the cells of lower SSC. This strategy has been

605   described to meet the demands of current T cell manufacturing procedures in both

606   quantity and quality (**Figures 4, S4, and S5**). A significantly higher yield of T cell with

607   more memory precursors can be achieved from the sorted SSC^{low} cell population. In

608   addition, a comparable amount of T cells with stronger immediate effector function due

36

609   to the production of late-differentiated effector cells, can also be obtained from the

610   SSC^{high} cluster when compared to unfractionated total lymphocytes. On the other hand,

611   the majority of NK cells can be assigned to SSC^{high} population, which would be useful

612   if antibody-free methods are preferred for NK cells segregation (Hu et al., 2019).

613

614   Apheresis materials with high baseline T cell dysfunction (LAG-3$^+$/TNF-α^{low} CD8$^+$ T)

615   before cell manufacturing was reported to correlate with the non-responding rate of B-

616   CLL patients while a more memory-like functional profile predicts better response

617   (Finney et al., 2019). Similarly, sustained disease remission in B-cell acute

618   lymphoblastic leukemia (B-ALL) patients was associated with memory-like CD27$^+$

619   CD45RO$^-$ CD8$^+$ T cells before CAR T engineering (Fraietta et al., 2018). Interestingly,

620   we observed that T cell progenies derived from SSC^{low} group have significantly

621   accumulated CD8$^+$ T$_{CMRA-hi}$ subpopulation, which is endowed with naïve-like cytokine

622   expression profile (**Figures 4G-4I, S5C, and S5D**) and increased co-stimulatory

623   markers CD27/CD28 but reduced CD45RO/LAG-3 especially during the early

624   expansion phases (**Figures 4F and S5B**). This finding is of great interest for further

625   studies. In addition, tumor histology heterogeneity (e.g. tumor burden and anatomic

626   distribution) and T cell immunosuppression/persistency mechanisms play important

627   roles in cancer immunity and treatment (Majzner and Mackall, 2019). Here we

628   conceive a sequential infusion regimen, that combines highly potential effector cells

629   (SSC^{high}-derived) to immediately mitigate tumor load and followed by less-

630   differentiated cells (SSC^{low}-derived) to improve long-term tumor surveillance. However,

631   it remains to be validated whether such a treatment regimen would be more efficacious

632   in refractory tumors aimed to maximally alleviate side effects (e.g. cytokine-releasing

633   syndrome and neurotoxicity) while preventing huge tumor burden-caused T cell over-

634   activation/exhaustion. The work has demonstrated its feasibility by producing

635   adequate cell doses but with distinctive cellular quality from one packet of apheresis

636   product.

637

638   Great efforts have been put into improving T cell manufacturing processes for better

639   immunotherapy. For example, shortening the time frame of T cell expansion from

640   around two weeks (Jacoby et al., 2019) to a few days (Ghassemi et al., 2018; Lu et al.,

641   2016; Tu et al., 2019) or even without expansion in so called FasT CAR-T technology

642   (Zhang et al., 2019). While more clinical data is required, both strategies have been

643   proposed to maximally maintain the younger T cell subpopulations with enhanced

644   engraftment and persistence. The use of homeostatic cytokine cocktails (e.g. IL-7/IL-

645   15) (Surh and Sprent, 2008) or antigen-specific stimulation to maintain pools of less-

646   differentiated T cells (e.g. T_{CM}/T_{SCM}) (Cieri et al., 2013; Xu et al., 2014) has also been

647   described. Additionally, CD4^{+} T or CD8^{+} T cells or CD8^{+} T_{CM} subset can be magnetically

648   pre-enriched and expanded separately in the presence of optimal cytokine cocktails,

649   and co-transfusion of CD4^{+} T and CD8^{+} T cell products has seen preliminary success

650   in both manufacturing and therapeutic studies (Gardner et al., 2017; Shah et al., 2020;

651   Sommermeyer et al., 2016; Turtle et al., 2016). CD4^{+} T help is critical for optimal CD8^{+}

652   T expansion and early central memory pool maintenance in the absence of specific

38

653   cognate antigens (**Figures 6 and 7**). Hence, it will be of great interest to study how the

654   pre-reconstituted CD4$^+$ T/CD8$^+$ T cells before expansion may further improve

655   therapeutic efficacy when combined with the defined ratio of CD4/CD8 T cells for

656   infusion. This would be more practically meaningful considering that patients with some

657   tumors or chronic diseases tend to manifest a decreased ratio of CD4/CD8 T cells

658   (Patel et al., 2016; Sommermeyer et al., 2016; You et al., 2009). On the other hand,

659   rapid expansion method (REM), which requires large amount of non-dividing feeder

660   cells such as irradiated allogeneic PBMC or antigen-bearing lymphoblastoid cell line

661   (LCL), has been used to quickly obtain large numbers of therapeutic T cells (Jin et al.,

662   2018; Wang and Riviere, 2015). Our findings would provide an alternative approach to

663   achieve this without the use of additional feeder cells where only a proper ratio of CD4$^+$

664   T to CD8$^+$ T cells is adopted for co-expansion. Given these research progresses, our

665   method can be flexibly adapted into those manufacturing workflows.

666

667   There are two main advantages for the technical feasibility of TRuST for the

668   preparation of clinical grade T cell products. (1) The lack of expensive staining reagents

669   can significantly reduce cost. By using only one laser (e.g. Blue laser 488 nm) for

670   generating forward-scatter and side-scatter, data-processing burden during real-time

671   sorting can also be simplified. (2) The successful application of good manufacturing

672   practice (GMP)-compliant multiparameter flow cytometry systems in cell therapy

673   (**Table   S1**) (Bluestone et al., 2015; Fritsche et al., 2020) and advances in microfluidic

674   systems enabling total lymphocytes enrichment immediately from whole blood in a

675   high-throughput approach by combining acoustic (Ding et al., 2013) and hydrodynamic

676   focusing (Lissandrello et al., 2018; Urbansky et al., 2017). Thus, we envisage the

677   versatility of side scatter-based lymphocytes analysis and reconstitution in these

678   platforms.

679

680   **Limitations**

681   Despite the simplicity and ingenuity associated with TRuST, a limitation of this strategy

682   is that it may not be feasible to discriminate differentiated lymphocyte subsets under

683   fast expansion due to confounding effects from enlarged cell size. A possible solution

684   could be the use of longer scattering wavelengths. Also, studies are required in future

685   to test how efficient the SSC-based lymphocyte segregation is when using patient

686   samples which usually manifest abnormal lymphocytes composition and activation

687   statuses. We have demonstrated that it is of adequate sensitivity and pronounced

688   usefulness to segregate the majority of naïve T cells from more-differentiated T cell

689   subsets with controllable CD4/CD8 T cells ratio. We have also showed that, it is

690   feasible to enhance the purification of specific lymphocyte subsets via computational

691   gate design. Nevertheless, it would be more powerful for other applications such as

692   label-free disease diagnosis and highly purified cell selection if the scattering resolution

693   was further improved with interdisciplinary efforts. For example, use of microchannel-

694   based fluidic systems and adoption of adjustable scattering angles (Rossi et al., 2019),

695   inclusion of generic dyes (e.g. MitoTracker) measuring mitochondrial

696   abundance/activity (Baron et al., 2019), or biomarkers possibly surrogating biophysical

697 properties (Tsai et al., 2020; Walsh et al., 2019) to improve lymphocyte subsets

698 identification.

699

700 Overall, TRuST is a reliable and effective approach for optimum T cell reconstitution,

701 that will be a significant improvement for current cell manufacturing methods. TRuST

702 is also feasible for the selection of specific lymphocyte subsets for lymphocyte biology

703 studies. This work has provided new insights into the intrinsic light-scattering attributes

704 of different lymphocytes and will pave the way for the improvement and broad

705 application of light property-relied cell identification and separation with

706 interdisciplinary efforts.

707

708 **SUPPLEMENTARY INFORMATION**

709 Supplementary information is available for this manuscript.

710

716

717 **AUTHOR CONTRIBUTIONS**

718 T.W and L.F.C conceived and designed the study. T.W performed the experiments and

719   data analysis with all other authors' assistance. T.W and L.F.C wrote the manuscript.

720   Y.H.L, Y.L, and H.J.W reviewed the manuscript and provided feedback. All authors

721   commented on the manuscript and approved the submission.

722

DECLARATION OF INTERESTS

724   The authors declare no competing interests.

725

REFERENCES

727   Alspach, E., Lussier, D.M., Miceli, A.P., Kizhvatov, I., DuPage, M., Luoma, A.M., Meng, W., Lichti,
728   C.F., Esaulova, E., Vomund, A.N., *et al.* (2019). MHC-II neoantigens shape tumour immunity and
729   response to immunotherapy. Nature *574*, 696-701.

730   Arina, A., Karrison, T., Galka, E., Schreiber, K., Weichselbaum, R.R., and Schreiber, H. (2017). Transfer
731   of Allogeneic CD4+ T Cells Rescues CD8+ T Cells in Anti-PD-L1-Resistant Tumors Leading to Tumor
732   Eradication. Cancer Immunol Res *5*, 127-136.

733   Attanasio, J., and Wherry, E.J. (2016). Costimulatory and Coinhibitory Receptor Pathways in Infectious
734   Disease. Immunity *44*, 1052-1068.

735   Baron, C.S., Barve, A., Muraro, M.J., van der Linden, R., Dharmadhikari, G., Lyubimova, A., de Koning,
736   E.J.P., and van Oudenaarden, A. (2019). Cell Type Purification by Single-Cell Transcriptome-Trained
737   Sorting. Cell *179*, 527-542 e519.

738   Berger, C., Jensen, M.C., Lansdorp, P.M., Gough, M., Elliott, C., and Riddell, S.R. (2008). Adoptive
739   transfer of effector CD8+ T cells derived from central memory cells establishes persistent T cell memory
740   in primates. J Clin Invest *118*, 294-305.

741   Bluestone, J.A., Buckner, J.H., Fitch, M., Gitelman, S.E., Gupta, S., Hellerstein, M.K., Herold, K.C.,
742   Lares, A., Lee, M.R., Li, K., *et al.* (2015). Type 1 diabetes immunotherapy using polyclonal regulatory
743   T cells. Science translational medicine *7*, 315ra189-315ra189.

744   Bohler, T., von Au, M., Klose, N., Muller, K., Coulibaly, B., Nauwelaers, F., Spengler, H.P., Kynast-Wolf,
745   G., and Krausslich, H.G. (2007). Evaluation of a simplified dual-platform flow cytometric method for
746   measurement of lymphocyte subsets and T-cell maturation phenotypes in the population of Nouna,
747   Burkina Faso. Clinical and vaccine immunology : CVI *14*, 775-781.

748   Chen, L., and Flies, D.B. (2013). Molecular mechanisms of T cell co-stimulation and co-inhibition. Nat
749   Rev Immunol *13*, 227-242.

750   Cieri, N., Camisa, B., Cocchiarella, F., Forcato, M., Oliveira, G., Provasi, E., Bondanza, A., Bordignon,
751   C., Peccatori, J., Ciceri, F., *et al.* (2013). IL-7 and IL-15 instruct the generation of human memory stem
752   T cells from naive precursors. Blood *121*, 573-584.

753   Clark, R.A., Shackelton, J.B., Watanabe, R., Calarese, A., Yamanaka, K., Campbell, J.J., Teague, J.E.,
754   Kuo, H.P., Hijnen, D., and Kupper, T.S. (2011). High-scatter T cells: a reliable biomarker for malignant

755   T cells in cutaneous T-cell lymphoma. Blood *117*, 1966-1976.

756   Cook, K.D., and Whitmire, J.K. (2013). The depletion of NK cells prevents T cell exhaustion to
757   efficiently control disseminating virus infection. Journal of immunology *190*, 641-649.

758   Cossarizza, A., Chang, H.-D., Radbruch, A., Acs, A., Adam, D., Adam-Klages, S., Agace, W.W.,
759   Aghaeepour, N., Akdis, M., Allez, M.*, et al.* (2019). Guidelines for the use of flow cytometry and cell
760   sorting in immunological studies (second edition). European journal of immunology *49*, 1457-1973.

761   Deng, Q., Han, G., Puebla-Osorio, N., Ma, M.C.J., Strati, P., Chasen, B., Dai, E., Dang, M., Jain, N.,
762   Yang, H.*, et al.* (2020). Characteristics of anti-CD19 CAR T cell infusion products associated with
763   efficacy and toxicity in patients with large B cell lymphomas. Nature medicine.

764   Denton, A.E., Russ, B.E., Doherty, P.C., Rao, S., and Turner, S.J. (2011). Differentiation-dependent
765   functional and epigenetic landscapes for cytokine genes in virus-specific CD8+ T cells. Proceedings of
766   the National Academy of Sciences of the United States of America *108*, 15306-15311.

767   Dimeloe, S., Mehling, M., Frick, C., Loeliger, J., Bantug, G.R., Sauder, U., Fischer, M., Belle, R.,
768   Develioglu, L., Tay, S.*, et al.* (2016). The Immune-Metabolic Basis of Effector Memory CD4+ T Cell
769   Function under Hypoxic Conditions. J Immunol *196*, 106-114.

770   Ding, X., Li, P., Lin, S.C., Stratton, Z.S., Nama, N., Guo, F., Slotcavage, D., Mao, X., Shi, J., Costanzo,
771   F.*, et al.* (2013). Surface acoustic wave microfluidics. Lab on a chip *13*, 3626-3649.

772   Finney, O.C., Brakke, H.M., Rawlings-Rhea, S., Hicks, R., Doolittle, D., Lopez, M., Futrell, R.B.,
773   Orentas, R.J., Li, D., Gardner, R.A.*, et al.* (2019). CD19 CAR T cell product and disease attributes predict
774   leukemia remission durability. J Clin Invest *129*, 2123-2132.

775   Fraietta, J.A., Lacey, S.F., Orlando, E.J., Pruteanu-Malinici, I., Gohil, M., Lundh, S., Boesteanu, A.C.,
776   Wang, Y., O'Connor, R.S., Hwang, W.T.*, et al.* (2018). Determinants of response and resistance to CD19
777   chimeric antigen receptor (CAR) T cell therapy of chronic lymphocytic leukemia. Nature medicine *24*,
778   563-571.

779   Fritsche, E., Volk, H.D., Reinke, P., and Abou-El-Enein, M. (2020). Toward an Optimized Process for
780   Clinical Manufacturing of CAR-Treg Cell Therapy. Trends Biotechnol *38*, 1099-1112.

781   Fuertes Marraco, S.A., Soneson, C., Cagnon, L., Gannon, P.O., Allard, M., Abed Maillard, S., Montandon,
782   N., Rufer, N., Waldvogel, S., Delorenzi, M.*, et al.* (2015). Long-lasting stem cell-like memory CD8+ T
783   cells with a naive-like profile upon yellow fever vaccination. Science translational medicine *7*, 282ra248.

784   Gardner, R.A., Finney, O., Annesley, C., Brakke, H., Summers, C., Leger, K., Bleakley, M., Brown, C.,
785   Mgebroff, S., Kelly-Spratt, K.S.*, et al.* (2017). Intent-to-treat leukemia remission by CD19 CAR T cells
786   of defined formulation and dose in children and young adults. Blood *129*, 3322-3331.

787   Gattinoni, L., Klebanoff, C.A., Palmer, D.C., Wrzesinski, C., Kerstann, K., Yu, Z., Finkelstein, S.E.,
788   Theoret, M.R., Rosenberg, S.A., and Restifo, N.P. (2005). Acquisition of full effector function in vitro
789   paradoxically impairs the in vivo antitumor efficacy of adoptively transferred CD8+ T cells. J Clin Invest
790   *115*, 1616-1626.

791   Gattinoni, L., Lugli, E., Ji, Y., Pos, Z., Paulos, C.M., Quigley, M.F., Almeida, J.R., Gostick, E., Yu, Z.,
792   Carpenito, C.*, et al.* (2011). A human memory T cell subset with stem cell-like properties. Nature
793   medicine *17*, 1290-1297.

794   Ghassemi, S., Nunez-Cruz, S., O'Connor, R.S., Fraietta, J.A., Patel, P.R., Scholler, J., Barrett, D.M.,
795   Lundh, S.M., Davis, M.M., Bedoya, F.*, et al.* (2018). Reducing Ex Vivo Culture Improves the
796   Antileukemic Activity of Chimeric Antigen Receptor (CAR) T Cells. Cancer Immunol Res *6*, 1100-1109.

797   Grutzkau, A., and Radbruch, A. (2010). Small but mighty: how the MACS-technology based on
798   nanosized superparamagnetic particles has helped to analyze the immune system within the last 20 years.

799   Cytometry A *77*, 643-647.

800   Hinrichs, C.S., Borman, Z.A., Cassard, L., Gattinoni, L., Spolski, R., Yu, Z., Sanchez-Perez, L., Muranski,

801   P., Kern, S.J., Logun, C*., et al.* (2009). Adoptively transferred effector cells derived from naive rather

802   than central memory CD8+ T cells mediate superior antitumor immunity. Proceedings of the National

803   Academy of Sciences of the United States of America *106*, 17469-17474.

804   Hinrichs, C.S., Borman, Z.A., Gattinoni, L., Yu, Z., Burns, W.R., Huang, J., Klebanoff, C.A., Johnson,

805   L.A., Kerkar, S.P., Yang, S*., et al.* (2011). Human effector CD8+ T cells derived from naive rather than

806   memory subsets possess superior traits for adoptive immunotherapy. Blood *117*, 808-814.

807   Hu, W., Wang, G., Huang, D., Sui, M., and Xu, Y. (2019). Cancer Immunotherapy Based on Natural

808   Killer Cells: Current Progress and New Opportunities. Frontiers in immunology *10*, 1205.

809   Jacoby, E., Shahani, S.A., and Shah, N.N. (2019). Updates on CAR T-cell therapy in B-cell malignancies.

810   Immunol Rev *290*, 39-59.

811   Jin, J., Gkitsas, N., Fellowes, V.S., Ren, J., Feldman, S.A., Hinrichs, C.S., Stroncek, D.F., and Highfill,

812   S.L. (2018). Enhanced clinical-scale manufacturing of TCR transduced T-cells using closed culture

813   system modules. Journal of translational medicine *16*, 13.

814   Klebanoff, C.A., Scott, C.D., Leonardi, A.J., Yamamoto, T.N., Cruz, A.C., Ouyang, C., Ramaswamy, M.,

815   Roychoudhuri, R., Ji, Y., Eil, R.L*., et al.* (2016). Memory T cell-driven differentiation of naive cells

816   impairs adoptive immunotherapy. J Clin Invest *126*, 318-334.

817   Laghmouchi, A., Hoogstraten, C., Falkenburg, J.H.F., and Jedema, I. (2020). Long-term in vitro

818   persistence of magnetic properties after magnetic bead-based cell separation of T cells. Scand J Immunol

819   *92*, e12924.

820   Lissandrello, C., Dubay, R., Kotz, K.T., and Fiering, J. (2018). Purification of Lymphocytes by Acoustic

821   Separation in Plastic Microchannels. SLAS Technol *23*, 352-363.

822   Loudon, W.G., Abraham, S.R., Owen-Schaub, L.B., Hemingway, L.L., Hemstreet, G.P., and DeBault,

823   L.E. (1988). Identification and selection of human lymphokine activated killer cell effectors and novel

824   recycling intermediates by unique light-scattering properties. Cancer Res *48*, 2184-2192.

825   Lu, T.L., Pugach, O., Somerville, R., Rosenberg, S.A., Kochenderfer, J.N., Better, M., and Feldman, S.A.

826   (2016). A Rapid Cell Expansion Process for Production of Engineered Autologous CAR-T Cell Therapies.

827   Human gene therapy methods *27*, 209-218.

828   Majzner, R.G., and Mackall, C.L. (2019). Clinical lessons learned from the first leg of the CAR T cell

829   journey. Nature medicine *25*, 1341-1355.

830   Nakanishi, Y., Lu, B., Gerard, C., and Iwasaki, A. (2009). CD8(+) T lymphocyte mobilization to virus-

831   infected tissue requires CD4(+) T-cell help. Nature *462*, 510-513.

832   Ojaghi, A., Carrazana, G., Caruso, C., Abbas, A., Myers, D.R., Lam, W.A., and Robles, F.E. (2020).

833   Label-free hematology analysis using deep-ultraviolet microscopy. Proceedings of the National Academy

834   of Sciences of the United States of America *117*, 14779-14789.

835   Patel, S., Jones, R.B., Nixon, D.F., and Bollard, C.M. (2016). T-cell therapies for HIV: Preclinical

836   successes and current clinical strategies. Cytotherapy *18*, 931-942.

837   Plouffe, B.D., Murthy, S.K., and Lewis, L.H. (2015). Fundamentals and application of magnetic particles

838   in cell isolation and enrichment: a review. Rep Prog Phys *78*, 016601.

839   Radtke, S., Pande, D., Cui, M., Perez, A.M., Chan, Y.-Y., Enstrom, M., Schmuck, S., Berger, A., Eunson,

840   T., Adair, J.E*., et al.* (2019). Sort-purification of human CD34+ CD90+ cells reduces target cell

841   population and improves lentiviral transduction. bioRxiv, 850479.

842   Rafiq, S., Hackett, C.S., and Brentjens, R.J. (2020). Engineering strategies to overcome the current

843   roadblocks in CAR T cell therapy. Nature reviews Clinical oncology *17*, 147-167.

844   Roddie, C., O'Reilly, M., Dias Alves Pinto, J., Vispute, K., and Lowdell, M. (2019). Manufacturing

845   chimeric antigen receptor T cells: issues and challenges. Cytotherapy *21*, 327-340.

846   Rossi, D., Dannhauser, D., Telesco, M., Netti, P.A., and Causa, F. (2019). CD4+ versus CD8+ T-

847   lymphocyte identification in an integrated microfluidic chip using light scattering and machine learning.

848   Lab on a chip *19*, 3888-3898.

849   Ruban, G.I., Berdnik, V.V., Marinitch, D.V., Goncharova, N.V., and Loiko, V.A. (2010). Light scattering

850   and morphology of the lymphocyte as applied to flow cytometry for distinguishing healthy and infected

851   individuals. J Biomed Opt *15*, 057008.

852   Schietinger, A., Philip, M., Liu, R.B., Schreiber, K., and Schreiber, H. (2010). Bystander killing of cancer

853   requires the cooperation of CD4(+) and CD8(+) T cells during the effector phase. The Journal of

854   experimental medicine *207*, 2469-2477.

855   Seder, R.A., and Ahmed, R. (2003). Similarities and differences in CD4+ and CD8+ effector and memory

856   T cell generation. Nature immunology *4*, 835-842.

857   Shah, N.N., Highfill, S.L., Shalabi, H., Yates, B., Jin, J., Wolters, P.L., Ombrello, A., Steinberg, S.M.,

858   Martin, S., Delbrook, C*., et al.* (2020). CD4/CD8 T-Cell Selection Affects Chimeric Antigen Receptor

859   (CAR) T-Cell Potency and Toxicity: Updated Results From a Phase I Anti-CD22 CAR T-Cell Trial. J

860   Clin Oncol *38*, 1938-1950.

861   Sommermeyer, D., Hudecek, M., Kosasih, P.L., Gogishvili, T., Maloney, D.G., Turtle, C.J., and Riddell,

862   S.R. (2016). Chimeric antigen receptor-modified T cells derived from defined CD8+ and CD4+ subsets

863   confer superior antitumor reactivity in vivo. Leukemia *30*, 492-500.

864   Stuart, T., Butler, A., Hoffman, P., Hafemeister, C., Papalexi, E., Mauck, W.M., 3rd, Hao, Y., Stoeckius,

865   M., Smibert, P., and Satija, R. (2019). Comprehensive Integration of Single-Cell Data. Cell *177*, 1888-

866   1902 e1821.

867   Sun, J.C., Williams, M.A., and Bevan, M.J. (2004). CD4+ T cells are required for the maintenance, not

868   programming, of memory CD8+ T cells after acute infection. Nature immunology *5*, 927-933.

869   Surh, C.D., and Sprent, J. (2008). Homeostasis of naive and memory T cells. Immunity *29*, 848-862.

870   Teeman, E., Shasha, C., Evans, J.E., and Krishnan, K.M. (2019). Intracellular dynamics of

871   superparamagnetic iron oxide nanoparticles for magnetic particle imaging. Nanoscale *11*, 7771-7780.

872   Terstappen, L.W., de Grooth, B.G., Nolten, G.M., ten Napel, C.H., van Berkel, W., and Greve, J. (1986a).

873   Physical discrimination between human T-lymphocyte subpopulations by means of light scattering,

874   revealing two populations of T8-positive cells. Cytometry *7*, 178-183.

875   Terstappen, L.W., De Grooth, B.G., Ten Napel, C.H., Van Berkel, W., and Greve, J. (1986b).

876   Discrimination of human cytotoxic lymphocytes from regulatory and B-lymphocytes by orthogonal light

877   scattering. J Immunol Methods *95*, 211-216.

878   Terstappen, L.W., de Grooth, B.G., van Berkel, W., ten Napel, C.H., and Greve, J. (1988). Application of

879   orthogonal light scattering for routine screening of lymphocyte samples. Cytometry *9*, 220-225.

880   Tsai, A.G., Glass, D.R., Juntilla, M., Hartmann, F.J., Oak, J.S., Fernandez-Pol, S., Ohgami, R.S., and

881   Bendall, S.C. (2020). Multiplexed single-cell morphometry for hematopathology diagnostics. Nat Med

882   *26*, 408-417.

883   Tu, S., Huang, R., Guo, Z., Deng, L., Song, C., Zhou, X., Yue, C., Zhang, L., He, Y., Yang, J*., et al.*

884   (2019). Shortening the ex vivo culture of CD19-specific CAR T-cells retains potent efficacy against acute

885   lymphoblastic leukemia without CAR T-cell-related encephalopathy syndrome or severe cytokine release

886   syndrome. American journal of hematology *94*, E322-E325.

887 Turtle, C.J., Hanafi, L.A., Berger, C., Gooley, T.A., Cherian, S., Hudecek, M., Sommermeyer, D.,
888 Melville, K., Pender, B., Budiarto, T.M., *et al.* (2016). CD19 CAR-T cells of defined CD4+:CD8+
889 composition in adult B cell ALL patients. J Clin Invest *126*, 2123-2138.

890 Urbansky, A., Ohlsson, P., Lenshof, A., Garofalo, F., Scheding, S., and Laurell, T. (2017). Rapid and
891 effective enrichment of mononuclear cells from blood using acoustophoresis. Sci Rep *7*, 17161.

892 van Leeuwen, E.M., Gamadia, L.E., Baars, P.A., Remmerswaal, E.B., ten Berge, I.J., and van Lier, R.A.
893 (2002). Proliferation requirements of cytomegalovirus-specific, effector-type human CD8+ T cells.
894 Journal of immunology *169*, 5838-5843.

895 Waller, E.C., McKinney, N., Hicks, R., Carmichael, A.J., Sissons, J.G., and Wills, M.R. (2007).
896 Differential costimulation through CD137 (4-1BB) restores proliferation of human virus-specific
897 "effector memory" (CD28(-) CD45RA(HI)) CD8(+) T cells. Blood *110*, 4360-4366.

898 Walsh, A., Mueller, K., Jones, I., Walsh, C.M., Piscopo, N., Niemi, N.N., Pagliarini, D.J., Saha, K., and
899 Skala, M.C. (2019). Label-free Method for Classification of T cell Activation. bioRxiv, 536813.

900 Wang, X., Berger, C., Wong, C.W., Forman, S.J., Riddell, S.R., and Jensen, M.C. (2011). Engraftment of
901 human central memory-derived effector CD8+ T cells in immunodeficient mice. Blood *117*, 1888-1898.

902 Wang, X., and Riviere, I. (2015). Manufacture of tumor- and virus-specific T lymphocytes for adoptive
903 cell therapies. Cancer Gene Ther *22*, 85-94.

904 Xu, Y., Zhang, M., Ramos, C.A., Durett, A., Liu, E., Dakhova, O., Liu, H., Creighton, C.J., Gee, A.P.,
905 Heslop, H.E.*, et al.* (2014). Closely related T-memory stem cells correlate with in vivo expansion of
906 CAR.CD19-T cells and are preserved by IL-7 and IL-15. Blood *123*, 3750-3759.

907 You, J., Zhuang, L., Zhang, Y.F., Chen, H.Y., Sriplung, H., Geater, A., Chongsuvivatwong, V., Piratvisuth,
908 T., McNeil, E., Yu, L.*, et al.* (2009). Peripheral T-lymphocyte subpopulations in different clinical stages
909 of chronic HBV infection correlate with HBV load. World J Gastroenterol *15*, 3382-3393.

910 Zeskind, B.J., Jordan, C.D., Timp, W., Trapani, L., Waller, G., Horodincu, V., Ehrlich, D.J., and
911 Matsudaira, P. (2007). Nucleic acid and protein mass mapping by live-cell deep-ultraviolet microscopy.
912 Nat Methods *4*, 567-569.

913 Zhang, C., He, J., Liu, L., Wang, J., Wang, S., Liu, L., Gao, L., Gao, L., Liu, Y., Kong, P.*, et al.* (2019).
914 CD19-Directed Fast CART Therapy for Relapsed/Refractory Acute Lymphoblastic Leukemia: From
915 Bench to Bedside. Blood *134*, 1340-1340.

916 Zhang, C., Wang, Z., Yang, Z., Wang, M., Li, S., Li, Y., Zhang, R., Xiong, Z., Wei, Z., Shen, J.*, et al.*
917 (2017). Phase I Escalating-Dose Trial of CAR-T Therapy Targeting CEA(+) Metastatic Colorectal
918 Cancers. Mol Ther *25*, 1248-1258.

919

METHODS

Reagents

922 Apheresis residual blood cones were collected from healthy adult donors from the

923 Health Sciences Authority (HSA), Singapore, with approval from Institutional Review

924 Board and informed consent from donors (NUS-IRB no. H-18-038E). Ficoll® Paque

925   Plus (GE Healthcare, 17-1440-02) was used for peripheral blood mononuclear cells

926   (PBMC) enrichment. Cell culture medium RPMI1640 (Gibco, A1049101)

927   supplemented with heat-inactivated fetal bovine serum (FBS) (Gibco, 10270106) was

928   used for primary cell culture. In some experiments, anti-CD3/CD28 Dynabeads^{TM}

929   (Gibco, 11161D) were used for T cell activation and expansion in the condition of

930   human recombinant IL-2 (Gibco, PHC0021) or where indicated, human recombinant

931   IL-7 plus IL-15. Phorbol ester (PMA) (Sigma-Aldrich, P8139) and ionomycin (Sigma-

932   Aldrich, I9657) were used for cell stimulation to produce cytokines. Cytofix/Cytoperm^{TM}

933   reagent kit (BD Biosciences, 554714) was used for cell fixation and permeabilization

934   before intracellular staining. Flow cytometry antibodies used in this study are listed as

935   follows. Antibodies from BD Biosciences include: CD3-BUV395 (Clone UCHT1; cat

936   #563546), CD4-BV786 (Clone SK3; cat #563877) and CD8-PE-Cy7 (Clone SK1; cat

937   #335787). Antibodies from Biolegend include: CD3-FITC (Clone UCHT1; cat #300406),

938   CCR7-PE (Clone G043H7; cat #353204), CD45RA-APC (Clone HI100; cat #304112),

939   CD45RO-Pacific Blue (Clone UCHL1; cat #304215),CD27-Pacific Blue (Clone M-T271;

940   cat #356413), CD28-FITC (Clone CD28.2; cat #302906), CD95-FITC (Clone DX2; cat

941   #305605), CD127-Brilliant Violet 785 (Clone A019D5; cat #351329), TIM-3-Pacific

942   Blue (Clone F38-2E2; cat #345041),   CD57-FITC (Clone HNK-1; cat #359603), LAG-

943   3-Brilliant Violet 785 (Clone 11C3C65; cat #369321) and human TruStain FcX reagent

944   (Cat #422302). Antibodies for intracellular staining include granzyme B-PE (BD

945   Biosciences, GB11; cat #561142), IFN-γ-FITC (Miltenyi Biotec, cat #130-090-433), IL-

946   2-PE (Miltenyi Biotec, cat #130-090-487) and TNF-α-APC (Miltenyi Biotec, cat #130-

947   091-267).

948

PBMC isolation and usage

950   PBMC were isolated from apheresis blood of healthy donors by density gradient

951   centrifugation. To ensure batch-to-batch consistency, the enriched PBMC were

952   counted and cryopreserved at 10 million cells/vial using liquid nitrogen and medium

953   containing 90% FBS and 10% DMSO. For each experiment, the cells were recovered

954   overnight in RPMI1640 supplemented with 10% FBS before downstream experiments.

955

T cell differentiation lineages and phenotypes characterization

957   In this study, two gating methods were used to identify T cell differentiation lineages.

958   For resting T cells, based on the expression level of canonical markers

959   CCR7/CD45RA/CD45RO, they can be broadly classified as naïve (T_N, CD45RA^{high}

960   CCR7^{high} CD45RO$^-$), central memory (T_{CM}, CD45RA$^{dim/-}$ CCR7^{low}), effector memory (T_{EM},

961   CD45RA$^{dim/-}$ CCR7$^-$) and terminally differentiated effector (T_{EMRA}, CD45RA^{high} CCR7$^-$)

962   (Bohler et al., 2007; Seder and Ahmed, 2003). For T cells undergoing activation and

963   proliferation, an in-depth gating strategy was adapted where the T_{CM} is further

964   dissected into naïve phenotype-closest CD45RA^{high} T_{CM} ($T_{CMRA-hi}$), memory phenotype-

965   closest CD45RA^{low} T_{CM} ($T_{CMRA-low}$) and CD45RA$^-$ T_{CM} (T_{CMO}), while T_{EM} with CD45RA

966   expression is classified into CD45RA^{low} T_{EM} ($T_{EMRA-low}$) and CD45RA^{high} T_{EM} ($T_{EMRA-hi}$).

967

968   To better understand the T cell dynamic changes in their activation/senescent statuses

48

969 either before or during expansion, the expression profile of a panel of selected cell

970 surface markers was longitudinally assessed, and it includes classical naïve/memory

971 markers CCR7/CD45RA/CD45RO, proliferation and survival-enhancing costimulatory

972 receptors CD27/CD28, and immune activation/inhibition markers

973 CD127/CD95/CD57/LAG-3/TIM-3. To mitigate compensation-induced mutual signaling

974 interferences in multiparameter flow cytometry, the staining panels were designed as

975 follows: panel for dynamic change of naïve/memory composition (CD3-FITC/CD4-

976 BV786/CD8-PE-Cy7/CCR7-PE/CD45RA-APC/CD45RO-V450), panel for co-

977 expression of co-stimulatory markers in naïve/memory subsets (CD3-BUV395/CD8-

978 PE.Cy7/CCR7-PE/CD45RA-APC/CD27-Pacific Blue/CD28-FITC), two panels were

979 designed for immune activation/inhibition markers profiling in naïve/memory T cell

980 subsets (CD3-BUV395/CD8-PE-Cy7/CCR7-PE/CD45RA-APC/CD45RO-Pacific Blue

981 /CD95-FITC/CD127-BV785, or CD3-BUV395/CD8-PE-Cy7/CCR7-PE/CD45RA-APC

982 /TIM-3-Pacific Blue/CD57-FITC/LAG-3-BV785). Pre-blocking step with TruStain FcX

983 (BioLegend) was included for all staining. For some experiments where significant

984 dead cells may be generated such as the first 2-3 days post T cell activation and PMA-

985 based stimulation, LIVE/DEAD viability dye (Invitrogen, L34963) was used to exclude

986 dead cells. CD3-FITC, CD4-BV786, and CD8-PE-Cy7 were from BD Biosciences. All

987 other antibodies used were purchased from BioLegend . Flow cytometry compensation

988 matrices and sample data acquisition were completed in CytoFLEX analyzer

989 (Beckman Coulter) and analyzed by FlowJo software version 10.

990

991 **Light-scattering distribution of lymphocytes**

992 To obtain the light-scattering profile of main lymphocyte populations and

993 subpopulations, PBMC were rested overnight, and stained with CD3-BUV395/CD4-

994 BV786/CD8-PE-Cy7 for T cell population identification, or CD3-BUV395/CD56-

995 BV786/CD19-FITC for NK and B cell identification, or CD3-BUV395/CD4-BV786/CD8-

996 PE-Cy7/CCR7-PE/CD45RA-APC for naïve/memory T cells characterization. After

997 washing, the cells were re-suspended in cold PBS before flow cytometry data

998 acquisition. For a label-free approach, the cells were washed twice in cold phosphate

999 buffer (PBS) before suspended in cold PBS and sorted on Moflo Astrios (Beckman

1000 Coulter). Sorted cells with different scattering intensity were stained to identify the

1001 percentages of CD3$^+$ CD4$^+$ T/CD3$^+$ CD8$^+$ T, NK/B cell, or T$_N$/T$_{CM}$/T$_{EM}$/T$_{EMRA}$. Where

1002 indicated, a panel of selected surface markers was included to probe the detailed

1003 activation/senescent phenotypes of sorted cell populations, including CD45RO, CD27,

1004 CD28, CD127, CD95, CD57, LAG-3 and TIM-3. The scattering plots were generated

1005 by FlowJo software.

1006

1007 **Lymphocytes enrichment by automatic gating search**

1008 Computational gating search (GateID) (Baron et al., 2019) was used to find the gate

1009 for optional cell type enrichment from a mixed cell population. Briefly, PBMC were

1010 recovered overnight and stained with different antibody panels for T cell identification

1011 (CD3-BUV395/CD4-BV786/CD8-PE-Cy7), NK/B cells identification (CD3-

1012 BUV395/CD56-BV786/CD19-FITC), or naïve/memory T cells characterization (CD3-

1013   BUV395/CD4-BV786/CD8-PE-Cy7/CCR7-PE/CD45RA-APC). After washing, flow

1014   cytometry data was acquired in CytoFLEX analyzer (Beckman Coulter). The raw

1015   readouts corresponding to FSC and SSC parameters for each cell type were exported

1016   and input into the GateID package. The yield for each desired cell type (e.g. CD4$^+$

1017   T/CD8$^+$ T/NK/B/T_N/T_{CM}/T_{EM}/T_{EMRA}) was set to 5% - 100 % and gating vertices were

1018   constantly set to 4. The yield is the count percentage of target cell type within the gating

1019   to that of the whole cell population, while the purity indicates the proportion of target

1020   cell type to total cell numbers within each gate corresponding to desired yield.

1021

1022   **Cell sorting**

1023   For light-scatter based label-free cell sorting from resting PBMC, cryopreserved PBMC

1024   were recovered overnight in RPMI1640 supplemented with 10% FBS and washed in

1025   cold phosphate buffer (PBS) before suspended in cold PBS and sorted on Moflo

1026   Astrios (Beckman Coulter). The excitation wavelength for the generation of side-

1027   scatter (488/6-nm filter) and forward-scatter (488/6-nm filter) was 488 nm. Where

1028   indicated, a combined excitation by 488 nm and 405 nm was adopted to sort

1029   lymphocytes of different side-scatter (488/6-nm and 405/10-nm filter). Side-scatter was

1030   measured at an orthogonal angle from the light beam propagation axis while forward-

1031   scatter was measured anti-parallel to the incident beam. To make batch-to-batch

1032   experiments comparable, the sorting gate was set to equally sort cell populations of

1033   different light intensity (SSC^{high}/SSC^{low} or FSC^{high}/FSC^{low}). For antibody staining-based

1034   cell sorting, PBMC were pre-blocked with TruStain FcX and stained with CD4-BV786

1035   (BD Biosciences) and CD8-PE-Cy7 (BD Biosciences) for sequential sorting of $CD4^+$

1036   cells and $CD8^+$ cells on Moflo Astrios. It is important to note that only the cells with the

1037   high expression of CD8 were sorted as $CD8^+$ T cells because there were some NK

1038   cells that also expressed diminished CD8. Also, anti-CD3 was not used for cell sorting

1039   experiments where the sorted cells would be subjected to CD3/CD28-engaged

1040   stimulation. The sorted cells were validated to achieve enough purity of $CD3^+$ $CD4^+$ T

1041   or $CD3^+$ $CD8^+$ T cells (> 97%) before reconstituted for co-culture assay.

1042

1043   **Cell stimulation and expansion in vitro**

1044   Sorted SSC^{low} and SSC^{high} cells were either expanded alone or reconstituted at a ratio

1045   of 1:1 (equal to total lymphocytes within initial cell sample) for co-expansion. The

1046   starting cell numbers for each condition were 0.08 million/well in 96-well plate. After 1-

1047   hour incubation at 37^oC, all cell groups were activated by CD3/CD28 engagement at

1048   anti-CD3/CD28 microbeads to cells ratio 3:1 and 5 ng/ml IL-2. Similarly, the sorted

1049 $CD4^+$ T cells and $CD8^+$ T cells were reconstituted at indicated ratios to achieve 0.06

1050   million/well. The ratio of anti-CD3/CD28 microbeads to cells was 3:1 and 5 ng/ml of IL-

1051   2 was supplemented. Half of the culture medium was replaced with fresh medium

1052   containing 5 ng/ml IL-2 every two days during initial activation/expansion stages (day

1053   3 to day 7) and daily during late expansion phases (day 7 to day 11). During the

1054   expansion course, the cell numbers in each group were counted by trypan blue

1055   exclusion and aliquoted into approximately 0.1 million/well for all groups to mitigate

1056   high cell concentration. Data collection included manual counting of total nucleated

1057   cells (TNC), flow cytometry detection of CD4/CD8 T cells, effector/memory

1058   composition, and effectors expression (e.g. cytokines and granzyme B) at indicated

1059   time points post activation.

1060

1061   Around 5 million expanded T cells at day 11 for each condition were cryopreserved for

1062   future usage. In some experiments where cell responsiveness to second stimulation

1063   was tested by CD3/CD28 engagement, the pre-expanded T cells at day 11 derived

1064   from different SSC groups were thawed and incubated at 37°C overnight. 0.06 million

1065   cells were seeded into each well of a 96-well plate and re-stimulated by anti-CD3/CD28

1066   microbeads at beads to cell ratio of 1:1 under 5 ng/ml IL-2 or 5 ng/ml IL-7 and 5 ng/ml

1067   IL-15. Total cell numbers were recorded by manual counting and split into

1068   approximately 0.1 million/well to minimize high cell concentration. To assess the ability

1069   of $CD4^+$ T cells to rescue the proliferation capability of extensively pre-expanded $CD8^+$

1070   T cells, cell materials derived from SSC^{high} group (day 13) which was enriched in large

1071   numbers of terminally differentiated $CD8^+$ T cells were labelled with CellTrace Far Red

1072   (Invitrogen, C34564) following the manufacturer protocol. The labelled T cells and

1073   sorted resting $CD4^+$ T cells of the same donor were reconstituted at indicated ratios

1074   and activated by anti-CD3/CD28 microbeads supplemented with 5 ng/ml IL-2. After 4

1075   days, total cell numbers were counted and stained with CD4-BV786 before analysis

1076   on flow cytometer to determine $CD8^+$ T cells proliferation.

1077

1078   **Functionality in effecting factors expression**

53

1079   To determine the immune response of T cells in cytokine and granzyme B expression,

1080   residual anti-CD3/CD28 microbeads were removed from expanded T cells at day 7 or

1081   day 11 before being re-stimulated in the presence or absence of 50 ng/ml PMA and 1

1082   µg/ml ionomycin for an additional 2.5 hours. Cells were collected and labelled with

1083   LIVE/DEAD viability dye before further blocking with TruStain FcX. Surface markers

1084   CD3-BUV395 and CD8-PE-Cy7 were used to characterize T cell populations. After

1085   fixation/permeabilization treatment, each sample was divided into two tubes for either

1086   cytokine detection with IFN-γ-FITC (Miltenyi Biotec), IL-2-PE (Miltenyi Biotec) and

1087   TNF-α-APC (Miltenyi Biotec) or granzyme B measurement with granzyme B-PE (BD

1088   Biosciences) where isotype control antibodies were properly included. Flow cytometry

1089   data were acquired in CytoFLEX analyzer (Beckman Coulter) and analyzed by FlowJo

1090   software. Notably, the CD4 marker has a substantial downregulation post PMA

1091   stimulation, thus the $CD3^+$ $CD8^-$ T cells were gated as $CD3^+CD4^+$ T cells instead for

1092   data presentation.

1093

1094   **Migration assay**

1095   *In vitro* chemotactic migration was used to evaluate the cells lymphnode-homing

1096   capacity. Briefly, CCL19 (300 ng/ml) and CCL21 (300 ng/ml) (PeproTech) in 100 µl

1097   culture medium were added to the lower chamber of 96-well transwell plate (5 µm

1098   porosity) (Corning, CLS3388). For control group, only culture medium without

1099   chemokines was added. 0.1 million expanded T cells (day 11) derived from SSC^{high},

1100 SSC^{low} and reconstituted $SSC^{high+low}$ groups, or from experiments using $CD4^+$ $T-CD8^+$

54

1101   T co-culture were seeded into the upper chamber in 80 µl culture medium. Each

1102   condition was conducted in duplicates. After five hours, the numbers of cells migrating

1103   to the lower chamber were counted by trypan blue exclusion. For migration capacity,

1104   the counts subtracted from the migrated cell numbers in control group were presented,

1105   correspondingly.

1106

1107   **Principal component analysis**

1108   For each cell sample derived from sorted SSC^{high}, SSC^{low} or reconstituted $SSC^{high+low}$

1109   population, the cell composition (T_N, $T_{CMRA-hi}$, $T_{CMRA-low}$, $T_{CMRA-low}$, T_{CMO}, T_{EM}, $T_{EMRA-hi}$,

1110   and $T_{EMRA-low}$) and multifunctional cytokine expression profile (IFN-γ^+ only, IL-2$^+$ only,

1111   TNF-α^+ only, IFN-γ^+ IL-2$^+$, IFN-γ^+ TNF-α^+, IL-2$^+$ TNF- α^+, and IFN-γ^+ IL-2$^+$ TNF-α^+) were

1112   integrated together for PCA calculation using the program embedded in Seurat

1113   package (Stuart et al., 2019). For PCA plotting, the same cell subsets from all groups

1114   with percentage less than 4% were omitted. The data for day 7 and day 11 were

1115   calculated separately. For data at day 7, the IFN-γ^+ IL-2$^+$/IFN-γ^+ TNF-α^+/IFN-γ^+ IL-2$^+$

1116   TNF-α^+ were combined as "IFN$^+$ Multi" due to relatively lower percentage of these cells

1117   in some donors expressing double positive cytokines.

1118

1119   **Statistical methods**

1120   All values with error bars are reported as mean ± SEM. Statistical analysis was

1121   performed using GraphPad Prism. Unpaired two-tailed *t*-test was used to evaluate

1122   statistical significances between two groups. Where indicated, paired two-tailed *t*-test

1123   was used to compare the differences between two groups that combined data of

1124   different donors together.

1125

1126   **DATA AND CODE AVAILABILITY**

1127   The data that support the findings of this study can be made available by the

1128   corresponding author. There is no customized code for this work. The set of adjustable

1129   parameters in GateID program has been indicated in the Methods section.

1130

1131